2013

The mechanism governing cutting of Polycrystalline Cubic Boron Nitride (PCBN) tool blanks with phase transformation induced fracture

Zhuoru Wu
Iowa State University

The mechanism governing cutting of Polycrystalline Cubic Boron Nitride (PCBN) tool blanks with phase transformation induced fracture

by

Zhuoru Wu

A thesis submitted to the graduate faculty

in partial fulfillment of the requirements for the degree of

MASTER OF SCIENCE

Major: Mechanical Engineering

Program of Study Committee:
Pranav Shrotriya , Major Professor
Palaniappa A. Molian
Baskar Ganapathysubramanian
Thomas J. Rudolphi
Frank E. Peters

Iowa State University

Ames, Iowa

2013

TABLE OF CONTENTS

ACKNOWLEDGEMENTS

I would like to thank my major professor, Dr. Pranav Shrotriya first for his support in every single aspect in my research. His patience, knowledge and encouraging style of research helped me a lot. I truly cherish the opportunity to work with him and feel very lucky to be his student.

I would like to thank Dr. Pal. Molian, the Co-advisor of my project, for providing me guidance in experimental aspect and training me of equipments. I would also like to thank Dr. Thomas Rudolphi, my committee members, for his guidance in the courses I took. In addition, thank Dr. Frank Peters and Dr.Baskar Ganapathysubramanian for their time being part of the committee and the evaluation process.

Thank Ammar Melaibari and Yixian Wang, for conducting the experiments and provide some of the testing data and result. Thank Diamond Innovations Inc. for donating the PCBN samples. Thank NSF for awarding the grant.

In addition, I would also like to thank my friends, colleagues, the department faculty and staff for making my time at Iowa State University a wonderful experience.

Finally, thanks to my parents for their constant encouragement and support.

ABSTRACT

The thesis presents a combined experimental and computational investigation of a novel thermochemical material removal mechanism for cutting of polycrystalline cubic boron nitride (PCBN) substrates through controlled crack propagation. The CO2-Laser/Waterjet machining system developed by the Iowa State University's Laboratory for Lasers, MEMS, and Nanotechnology was utilized to achieve specimen cutting. It has been proved that the hybrid machining method is more efficiency and able to provide high quality cutting that overcomes the major drawbacks with current EDM and Nd:YAG laser machining techniques. The LWJ method implemented a high power laser heating followed by low pressure waterjet quenching that achieved fracture initiation and propagation along the cutting path. The purposes of water in LWJ machining are: (1) help the phase transformation as to induce larger tensile stresses for crack propagation and (2) provide thermal shock that reduce the fracture toughness of material in specimen. Two forms of PCBN specimens: the solid compact and the composite with tungsten carbide substrate were studied in this thesis. The mechanism governing the fracture behavior was studied through Raman spectroscopy, Scanning Electron Microscopy (SEM), and surface profile measurement with profilometer. FEA model associated with machining parameters was developed to validate the machining mechanism and provide prediction of fracture behavior. Good agreement between simulation prediction and experimental observation was achieved.

CHAPTER I

INTRODUCTION

1.1 Introduction to Polycrystalline Cubic Boron Nitride (PCBN)

Cubic Boron Nitride (cBN) is the second hardest material on earth, inferior only to diamond. It is not found in nature but can be synthesized by application of high temperature and pressure[1]. Polycrystalline cubic boron nitride (PCBN) blank are produced through sintering of CBN powders with ceramic matrix such as titanium nitride (TiN) or aluminum nitride (AlN). Since its discovery, PCBN has been used in industry as a substitute for diamond due to the superior thermal and chemical stability. The advantages that PCBN does not react with ferrous metals and has a high resistance to oxidation[2] makes it ideal tool material for machining hard cast iron, high chrome alloy steels, high-strength nickel super alloys, powder metal alloys and metal matrix composites[3].

Boron nitride exits four main phases: hexagonal (hBN), rhombohedral (rBN), cubic zincblende (cBN), and wurtzite (wBN) phases. The cBN and wBN phases are diamond-like sp3 bonded phases and hBN and rBN phases are graphite-like sp2 phases. The stable phases at ambient conditions are cBN and hBN structure while rBN and wBN are metastable phases that cannot last for a long time. Transformation between these phases would happen under high temperature or high pressure[4]. It was reported that the sp2-bonded structure occupies much more volume than sp3-bonded structure[5].

PCBN tool blanks are usually available in two forms: a solid compact or a composite with tungsten carbide substrate. While PCBN offers high wear resistance during machining, carbide substrates offer the required toughness as well as low cost making the composite

tools an ideal choice for manufacturers. PCBN blanks in the thickness range 1.6 mm to 4.8 mm are available to making inserts in the form of rounds, squares, diamonds, and triangles designed to fit special usage in different industries. The tool inserts are initially cut from PCBN wafer into small pieces and post processing such as grinding and polishing are needed to make them into the final product (Figure 1.1).

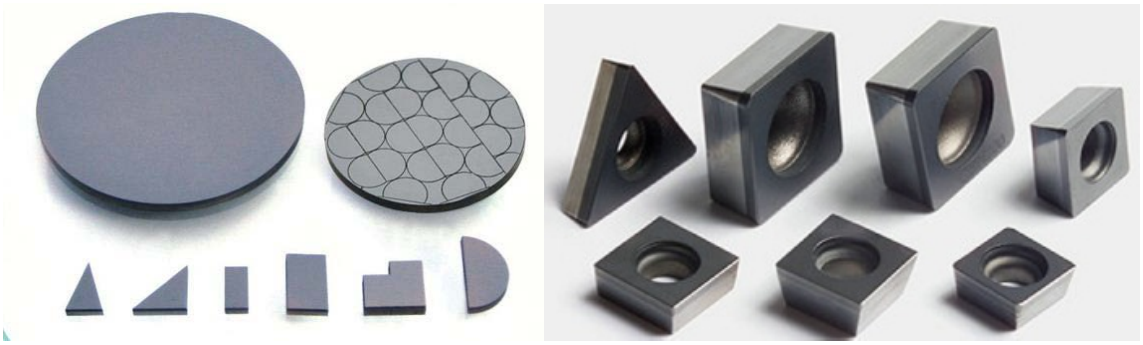

Figure 1.1. *Demonstration of PCBN blanks and tool inserts*

1.2 Current machining techniques

Due to the extreme hardness, it is difficult to machine the PCBN tool blanks. CBN tool inserts are traditionally cut from the compact blanks by either diamond sawing, electric discharge machining (EDM) or Nd:YAG laser cutting and finished by diamond grinding, lapping, and polishing. In tool production, high speed, low cost and fine resolution are the main consideration for industrial productivity. Diamond saw is not acceptable due to rapid tool wear and slowness of the process. In addition, small kerfs are difficult to produce due to blade thickness. Electric discharge machining (EDM) [6, 7] and electric discharge grinding (EDG) [8, 9] of PCD are constrained by high machining cost, slowness and low efficiency. EDM cannot be used if the compact is not electrically conductive (example: PCBN with AlN binder). Conventional Nd:YAG laser cutting suffers from particle formation (due to

vaporization) and thermal damages, conical kerfs and post processing becomes essential. Therefore, none of the current machining processes perform a favorable job due to the extreme hardness of PCBN materials. Traditional manufacturing methods for producing tool inserts in PCBN are slow and cost-inefficient.

Given the limitations of conventional material removal mechanisms, a number of recent reports have focused on non-conventional mechanisms for cutting and machining of PCBN. Hidai and Tokura [10] investigated the hydrothermal-reaction assisted laser drilling of PCBN in steam environment based on measurements of mass loss at high temperatures. CBN film deposited on copper substrate, binder-containing sintered PCBN, and binderless sintered PCBN were irradiated with an Ar-ion laser in water and steam as well as in different gas atmospheres. Single-crystal and binderless sintered CBN reacted very well with steam and thus hydrothermal-reaction-assisted laser machining was effective. However the technique failed in machining the binder-containing sintered CBN.

Water jet-guided laser technology[11] - also known as Laser MicroJet® developed by researchers in Swiss Federal Institute of Technology was an innovative technology that allows precise cutting of PCBN materials with smaller kerf and good surface finish. The concept of this technology is to focus a laser beam into a nozzle while passing through a pressurized water chamber. The free laminar waterjet is used as an optical waveguide to direct the Nd:YAG laser beam onto the sample. A Q-switched pulse laser (up to 300 W) of 532 nm wavelength and water pressure of 2-10 MPa was employed for the process. The waterjet permitted parallel beam transmission through the sample leading to taper-free and narrow kerf features. The tolerances are much smaller than those obtained with conventional laser and EDM processes. However the process suffers from very slow cutting speeds as it

reports 120 passes with each pass at a speed of 25mm/s were needed to cut 1.6mm WC supported PCBN sample.

1.3 Innovative Laser/Waterjet(LWJ) technique

Given to the limitation of existing machining method of PCBN, a novel process of combining continuous wave CO2 laser and water-jet (LWJ) was developed by our group to improve the machining efficiency and quality of PCBN. The CO2-LWJ machining system (schematically shown in Figure 1.2) implemented a high power laser heating followed by low pressure waterjet quenching that achieved fracture initiation and controlled propagation along the cutting path.

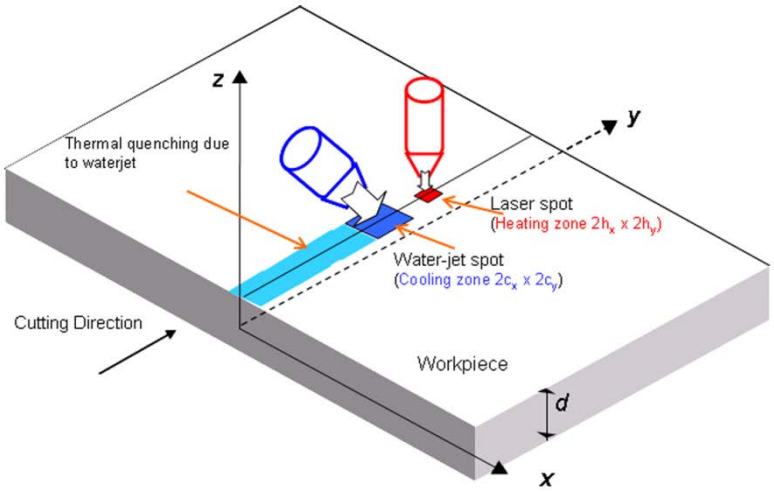

Figure 1.2. *Schematic representation of CO2-LWJ machining system*

The experimental setup of the LWJ system is represented in Figure 1.3 and the working principles has been previously reported [12-15]. A continuous wave CO2 Laser (Model 820 Spectra Physics) of 10.6 μm wavelength and 1.5 kW rated power was used in the

LWJ system. The laser head has been modified to accommodate the low-pressure waterjet (< 1000psi or < 8MPa) to realize CO2-LWJ machining. A CNC table with freedom in horizontal plane was implemented to control the movement of sample mounted on it. The beam from the laser was sent through a focusing lens and irradiated on the sample surface. A 127 mm focal length lens was used to produce the focal spot diameter of 0.2 mm. A defocused spot with diameter larger than 0.2mm can be achieved through adjusting the distance between laser head and sample surface. The distance between water jet and laser beam was determined from the location of spray hole for water on the laser nozzles. Three nozzles with spacing of 2 mm, 4mm and 6mm between water and laser was manufactured. Laser beam was surrounded by gases with a designed pressure in order to prevent direct interaction of laser and water jet.

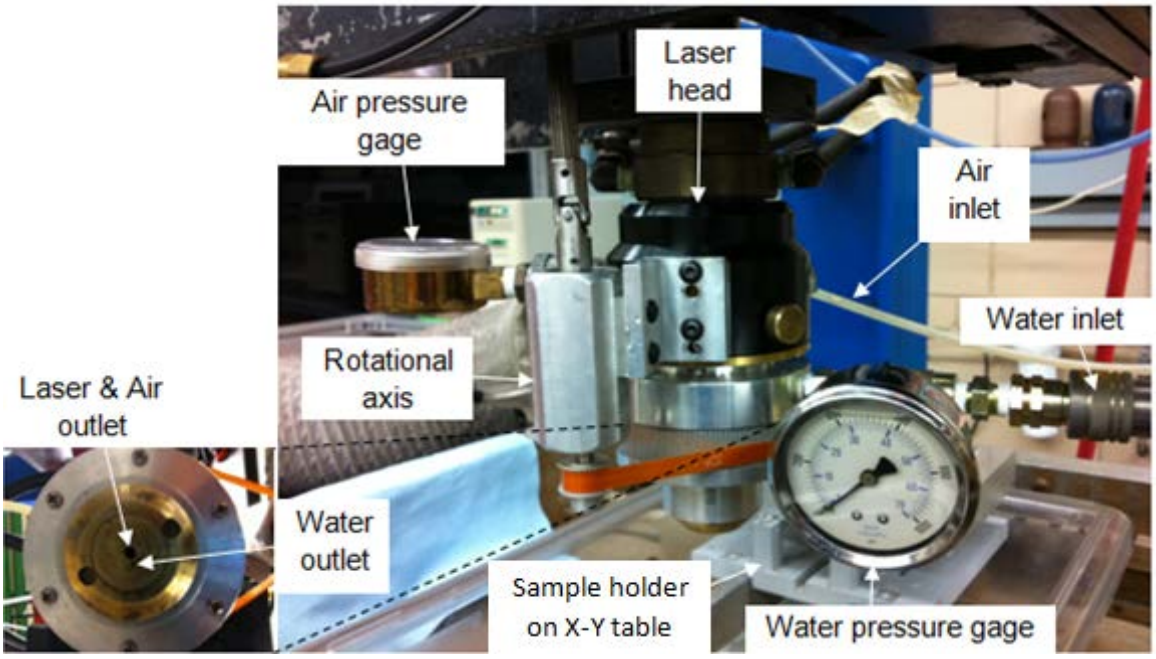

Figure 1.3. *Experimental setup of CO2-LWJ machining system*

The LWJ machining method uses an entirely different mechanism than conventional laser machining of material removal through melting and ablation. It achieved the material separation through controlled crack propagation which will be much faster and free of heat affected zone. In previous study of cutting of brittle ceramics with low thermal conductivities such as AlN and Alumina[14], the main source that induced fracture propagation was the thermal stress generated from rapid laser heating and water-jet quenching on the sample surface layer. While in cutting of high thermal conductive PCBN, the temperature gradient will be insignificant that induce no much thermal stresses. The main driven force for machining PCBN was the stresses induced by volume change in the transformed material. The volumetric change initiates a tensile stress field underneath the transformation region that induced the initial crack that propagated through the whole thickness and separated the material.

This controlled fracture mechanism offers a fast, cheap, and low energy method to cut difficult-to-machine materials like PCBN and PCD. Different fluid media beyond waterjet were investigated in previous study in our group[16] and waterjet was reported to be the best one for machining of PCBN.

1.4 Thesis organization

Chapter 1 provides the background information of the machined material (PCBN), the motivation for the studies and the introduction of current LWJ machining system. Chapter 2 investigated the cutting experiments and analytical approach to identify the mechanism

governing the cutting of solid PCBN sample by the single-pass LWJ manufacturing process. Chapter 3 analyzed the cutting of double-layer composite PCBN supported by tungsten carbide. A new method that combining single-pass focused beam and multi-passes defocused beam was applied that successfully achieved separation of the specimen. Chapter 4 presented the general conclusions of the studies in chapters 2 and 3 and described the future works.

1.5 References

[1] R. H. Wentorf, "Synthesis of Cubic Form of Boron Nitride," Journal of Chemical Physics, vol. 34, pp. 809-&, 1961.

[2] P. B. Mirkarimi, K. F. McCarty, and D. L. Medlin, "Review of advances in cubic boron nitride film synthesis," Materials Science & Engineering R-Reports, vol. 21, pp. 47-100, Dec 15 1997.

[3] X. Ding, W. Y. H. Liew, and X. D. Liu, "Evaluation of machining performance of MMC with PCBN and PCD tools," Wear, vol. 259, pp. 1225-1234, 2005.

[4] H. Sachdev, R. Haubner, H. Noth, and B. Lux, "Investigation of the cBN/h-BN phase transformation at normal pressure," Diamond and Related Materials, vol. 6, pp. 286-292, Mar 1997.

[5] J. Robertson, "Diamond-like amorphous carbon," Materials Science & Engineering R-Reports, vol. 37, pp. 129-281, May 24 2002.

[6] Y. H. Liu, Y. F. Guo, and J. C. Liu, "Electric discharge milling of polycrystalline diamond," Proceedings of the Institution of Mechanical Engineers Part B-Journal of Engineering Manufacture, vol. 211, pp. 643-647, 1997.

[7] P. L. Tso and Y. G. Liu, "Study on PCD machining," International Journal of Machine Tools & Manufacture, vol. 42, pp. 331-334, Feb 2002.

[8] X. L. Liu, Y. F. Li, F. G. Yan, Y. Wang, J. S. Hu, and Y. J. Wang, "Study on precision grinding technique of PCD tool's cutting edge," in Advances in Grinding and Abrasive Technology Xiii. vol. 304-305, ed, 2006, pp. 186-190.

[9] J. Y. Pei, C. N. Guo, and D. J. Hu, "Electrical discharge grinding of polycrystalline diamond," in Advances in Materials Manufacturing Science and Technology. vol. 471-472, ed, 2004, pp. 457-461.

[10] H. Hidai and H. Tokura, "Hydrothermal-reaction-assisted laser machining of cubic boron nitride," Journal of the American Ceramic Society, vol. 89, pp. 1621-1623, May 2006.

[11] A. Pauchard, M. D. Marco, B. Carron, G. Suruceanu, B. Richerzhagen, A. Brulé, et al., "Recent Developments in the Cutting of Ultra Hard Materials Using Water Jet-Guided Laser Technology," presented at the ALAC, 2008.

[12] D. Kalyanasundaram, G. Shehata, C. Neumann, P. Shrotriya, and P. Molian, "Design and validation of a hybrid laser/water-jet machining system for brittle materials," Journal of Laser Applications, vol. 20, pp. 127-134, May 2008.

[13] D. Kalyanasundaram, P. Shrotriya, and P. Molian, "Obtaining a relationship between Process parameters and Fracture energy for CO2 Laser/Waterjet Machining of Ceramics," Journal of Engineering Materials and Technology, vol. 131, pp. 011005-10, 2009.

[14] C. Barnes, P. Shrotriya, and P. Molian, "Water-assisted laser thermal shock machining of alumina," International Journal of Machine Tools & Manufacture, vol. 47, pp. 1864-1874, Oct 2007.

[15] D. Kalyana-sundaram, J. Wille, P. Shrotriya, and P. Molian. (2008). CO2 Laser/Waterjet machining of Polycrystalline Cubic Boron Nitride.

[16] A. Melaibari, P. Molian, and P. Shrotriya, "Effect of Fluid Medium on Laser Machining of Polycrystalline Cubic Boron Nitride Tool," presented at the The 44th CIRP Conference on Manufacturing Systems, 2011.

CHAPTER II

THE MECHANISM GOVERNING CUTTING OF POLYCRYSTALLINE CUBIC BORON NITRIDE (PCBN) WITH TRANSFORMATION INDUCED FRACTURE

A paper prepared for *International Journal of Machine Tools and Manufacture*

Zhuoru Wu, Ammar Melaibari, Pal Molian and Pranav Shrotriya

Abstract

A combined experimental and analytical approach is undertaken to identify mechanism governing the cutting of polycrystalline Cubic Boron Nitride (PCBN) sample by a hybrid CO2 laser/waterjet (CO2-LWJ) manufacturing process. In CO2-LWJ machining, a high power laser was used for local heating followed by waterjet quenching of the sample surface leading to fracture propagation along the sample surface. Cutting results indicate two fracture behaviors: scribing and through fracture. Raman spectroscopy analysis of the cut surface indicates that laser heated PCBN undergoes chemical phase transformation from sp3-bonded cubic Boron Nitride (cBN) into hexagonal Boron Nitride (hBN) and other sp2-bonded phases. Surface profile was experimentally measured using profilometer and compared with analytical predictions in order to estimate the expansion strain and dimensions of transformation region associated with CO2-LWJ induced transformation. FEM calculation was used to determine stress fields generated in the workpiece based on the strain and volume measured experimentally in order to determine the feasibility of crack propagation.

KEYWORDS: Laser/waterjet machining (LWJ), cubic boron nitride, phase transformation, crack propagation

2.1 Introduction

Cubic Boron Nitride (cBN) is the second hardest material on earth, inferior only to diamond. It is not found in nature but can be synthesized by application of high temperature and pressure [1]. Polycrystalline cubic boron nitride (PCBN) blank are produced through sintering of CBN powders with ceramic matrix such as titanium nitride (TiN) or aluminum nitride (AlN). Since its discovery, PCBN has been used in industry as a substitute for diamond due to the superior thermal and chemical stability. The advantages that PCBN does not react with ferrous metals and has a high resistance to oxidation[2] makes it ideal tool material for machining hard cast iron, high chrome alloy steels, high-strength nickel super alloys, powder metal alloys and metal matrix composites[3].

CBN Tool inserts are traditionally cut from the compact blanks by either diamond sawing, electric discharge machining (EDM) or Nd:YAG laser cutting and finished by diamond grinding, lapping, and polishing. A variety of tool geometries such as square, triangle, circle and rhombus are fabricated for use in various machining operations. The main requirements of a manufacturing process in cutting the desired geometry of tool inserts are: capabilities to generate smooth surface, parallel and narrow kerf, minimal heat affected zone and excellent dimensional tolerance enabling precision; and high cutting speed. In tool production, high speed, low cost and fine resolution are the main consideration for industrial productivity. However, none of the current machining processes perform the combination of these features due to the extreme hardness of PCBN materials. Traditional manufacturing methods for producing tool inserts in PCBN are slow and cost-inefficient.

Given the limitations of conventional material removal mechanisms, a number of recent reports have focused on non-conventional mechanisms for cutting and machining of PCBN. Hidai and Tokura [4] investigated the hydrothermal-reaction assisted laser drilling of PCBN in steam environment based on measurements of mass loss at high temperatures. CBN film deposited on copper substrate, binder-containing sintered PCBN, and binderless sintered PCBN were irradiated with an Ar-ion laser in water and steam as well as in different gas atmospheres. Single-crystal and binderless sintered CBN reacted very well with steam and thus hydrothermal-reaction-assisted laser machining was effective. However the technique failed in machining the binder-containing sintered CBN.

Swiss Federal Institute of Technology in Lausanne, Switzerland has developed Laser-Microjet® [5], a hybrid technology based on waterjet-guided Nd:YAG laser for machining of PCBN. In this unique laser cutting technique, a free laminar waterjet is used as an optical waveguide to direct the Nd:YAG laser beam onto the sample. The Laser-Microjet® allows precise cutting of PCBN materials with smaller kerf and better surface finish. A Q-switched pulse laser (up to 300 W) of 532 nm wavelength and water pressure of 2-10 MPa was employed for the process. The waterjet prevented any thermal damage and permitted parallel beam transmission through the sample leading to taper-free and narrow kerf features. The tolerances are much smaller than those obtained with conventional laser and EDM processes. However the process suffers from very slow cutting speeds as it reports 70 passes with each pass at a speed of 7 mm/min to cut 3.25 mm thick PCBN sample.

Crack propagation provides an energy and cost efficient method for cutting of ceramics because hardness and brittleness of ceramics lead to low material removal rates and slow cutting speeds during conventional machining processes. In low thermal conductivity

ceramics such as alumina thermal shock induced fracture has been successfully utilized for energy efficient cutting [6, 7]. However in high thermal conductivity ceramics such as polycrystalline cubic boron nitride (PCBN), thermal shock is not feasible. In this paper, we investigate fracture based material separation of PCBN due to synergistic interactions between laser heating and subsequent waterjet quenching through "score and snap" mechanism — laser heating leads to localized damage and oxidation of surface layers; and subsequently, stress fields developed due to constrained expansion of transformed material and waterjet quenching act on the laser-produced "score" to propagate crack through the thickness. A CO2-Laser/waterjet machining (CO2-LWJ) [6-9] system was used to investigate a novel mechanism for cutting of PCBN compacts through controlled fracture rather than energy intensive erosion or ablation of material. Cut surfaces were analyzed to identify the mechanism governing material separation. Stress fields induced due to volumetric expansion associated with oxidation of PCBN and binder were determined.

2.2 Experimental procedure

A continuous wave CO2 Laser (Model 820 Spectra Physics) of 10.6 μm wavelength and 1.5 kW rated power was used for the experiments. The laser head has been modified to accommodate the low-pressure waterjet (< 1000psi or < 8MPa) to realize CO2-LWJ machining. The working principle of the CO2-LWJ system is presented in Figure 2.1 and has been previously reported [6-8]. The workpiece is irradiated with a CO2 laser beam for localized heating and subsequently, the heated spot is rapidly quenched with the trailing waterjet.

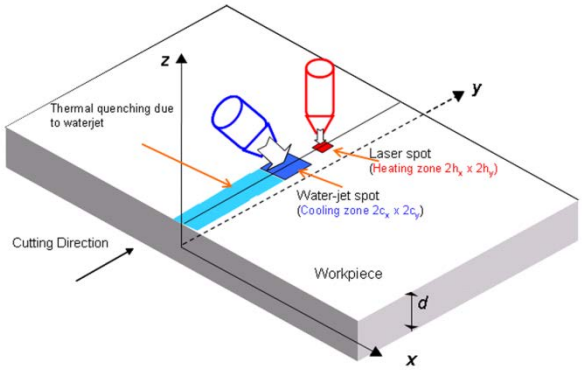

Figure 2.1. *Schematic representation of CO2-LWJ machining setup*

CO2-LaserWaterjet cutting experiments were carried on the commercial Polycrystalline Cubic Boron Nitride (PCBN) produced by Diamond Innovations, Inc. (Worthington, Ohio). Two different sets of experiments were performed on PCBN samples: the first set was conducted to determine the effect of processing parameters on the fracture behavior; the other set was conducted to obtain the size of phase transformed zone as well as the expansion strain associated with machining. The sample in first set was a triangular PCBN insert with dimension of 7mm side length and 1.6mm thickness. It is a member of BZN 7000 series with a composition of 82% CBN/ceramic (average particle size of 15 μm) and other impurities containing carbon. Surface roughness (Ra) was 0.3μm of the polished faces and 3μm of the side. The sample used in the second set was 4.8mm in thickness.

Laser beam was focused on the sample surface to a spot size of 0.2mm using a 127mm (5 in.) focal length lens. Pressure of water-jet was maintained at 800 psi as to apply rapid quenching on the heated region. The distance between laser beam and water-jet was set up to be 2mm to prevent direct interaction between them. During the experiments, laser beam was irradiated outside the PCBN sample, then translated into it and stopped out of the other

side. After each cutting test, the sample surface was carefully examined and characterized based on the fracture behaviors.

It has been shown in our previous publications that the different fracture behavior of LWJ machining of alumina[8] was a function of line energy (ratio of laser power to cutting velocity). Therefore, the aim of the first set of cutting experiments was to study how the crack behavior affected by the line energy (P/v) in PCBN sample. Three single pass cuttings were carried out with different cutting speed at laser power of 500W. The details of cutting parameters are shown in Table 2.1.

Table 2.1. *Parameters of experiment set 1*

Number of cutting	Cutting speed(in/min)	Power(W)	Line Energy P/v(kJ/m)
1	50	500	23.6
2	100	500	11.8
3	200	500	5.9

The second set of cutting was conducted for measuring expansion strain due to phase transformation and predicting dimensions of the phase transformation zone. Thick specimen was used to generate distinct surface scribing without material separation. Three single pass cuttings were carried out with parameters given in Table 2.2. Surface profiles around each scribing line were measured using optical profilometer (Zygo NewView 7100) and statistical analysis was applied on these data aim to reduce variance. The measured surface profiles cut by different line energy values were compared with FEM displacement result calculated from different expansion strain values and various dimensions of transformed zone. The best

match result indicated the actual expansion strain and revealed the relationship between line energy and dimensions (depth and width) of transformation region.

Table 2.2. *Parameters of experiment set 2*

Number of cutting	Cutting speed(in/min)	Power(W)	Line Energy P/v(kJ/m)
1	50	800	37.8
2	100	800	18.9
3	200	800	9.4

After the cutting experiments, scanning electron microscopy (SEM Model JEOL JSM-606LV at 20 kV) was used to inspect the cut surface in order to identify the depth of transformation zone. Raman spectroscopy (Renishaw-inVia Raman Microscopy) with Ar-ion laser at a wavelength of 488nm was utilized to identify the phases present in the laser irradiated zone.

2.3 Numerical modeling

2.3.1 Finite element analysis for determination of transformation induced stress field

Similar to carbon, boron nitride exits both diamond-like sp3 bonded phases(cBN and wBN) and graphite-like sp2 phases (hBN and rBN) and transformation between these phases would happen under high temperature or high pressure conditions[10]. It was reported that the sp2-bonded structure occupies much more volume than sp3-bonded structure[11], therefore transformed material has an tendency to expand the original material. Based on experimental observations of cutting and Raman analysis of cut surfaces, we hypothesize that

laser irradiated zone of the PCBN workpiece undergoes a phase transformation during cutting process that results in volume expansion of the transformed region. The volumetric change initiates a tensile stress field in the surrounding material that lead to propagation of crack through thickness direction. The hypothesis of the crack propagation mechanism is schematically represented in Figure 2.2. A finite element model is developed to investigate the validity of the proposed hypothesis.

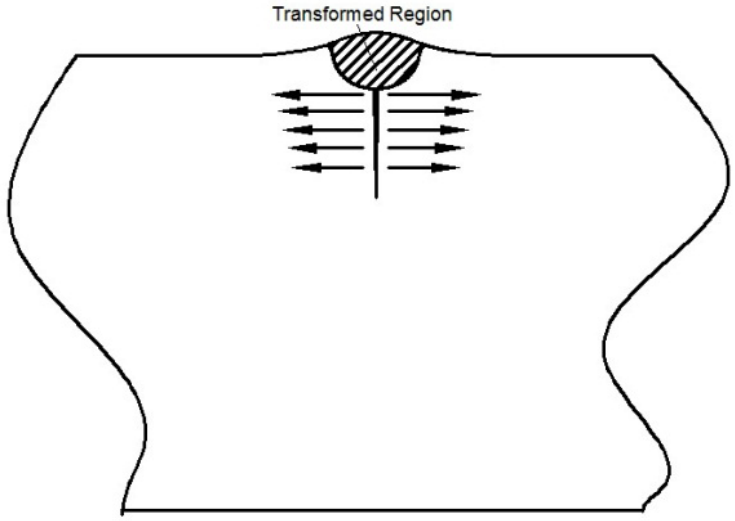

Figure 2.2. *Hypothesis for Crack propagation mechanism*

The PCBN workpiece subjected CO2-LWJ machining was modeled in finite element analysis package ABAQUS (Simulia, Providence, RI). A transformation zone undergoing uniform expansion was utilized to model the influence of material transformation along the cutting path. Material inside the transformation zone was applied the properties of h-BN while material outside it was initial PCBN. Volume of the transformed material will be estimated based on the comparison of predicted surface deformation and experimental

measurements. Cross-section of the transformation region was modeled as a semi-ellipse since laser intensity follows a Gaussian distribution. A schematic diagram of the finite element model of the workpiece indicating the transformed zone is presented in Figure 2.3. Due to the symmetry, only one half of the workpiece was analyzed with fixed boundary condition on the axis of symmetry. Fixed boundary condition in vertical direction was applied on outer edge to simulate the support of the table. The dimensions of the transformation zone in XZ plane (comparable to laser spot size ~ 0.1mm) are significantly smaller than the length along laser path direction (comparable to sample size ~ cm). Therefore plane strain state can be applied to this model to obtain stress field in XZ plane.

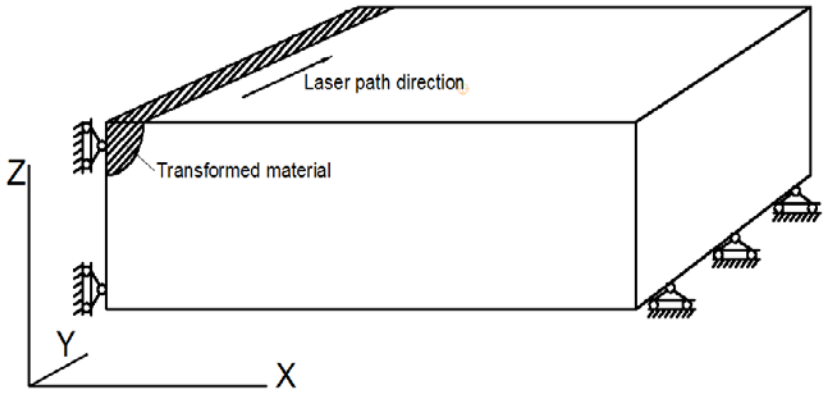

Figure 2.3. *Finite Element model and boundary conditions*

2.3.2 Fracture mechanics analysis of crack

Fracture mechanics analysis based on energy criterion was performed to determine the crack propagation behavior for particular line energy of CO2-LWJ machining. Laser irradiation caused the non-stable phase transformation which lead to crack nucleation and propagate under transformation stress towards both thickness direction and laser moving

direction. This phenomenon indicated two kinds of crack configurations: plane strain crack through vertical direction and channeling crack along laser path (schematically represented in Figure 2.4). At the beginning of a cut, laser beam was irradiated outside the sample, then moved in and created a crack at the edge across the thickness. This crack was a plane strain crack which may be utilized to estimate initial cut depth. As the laser went further, the existing plane strain crack propagated following the laser path which was considered to be the channeling crack.

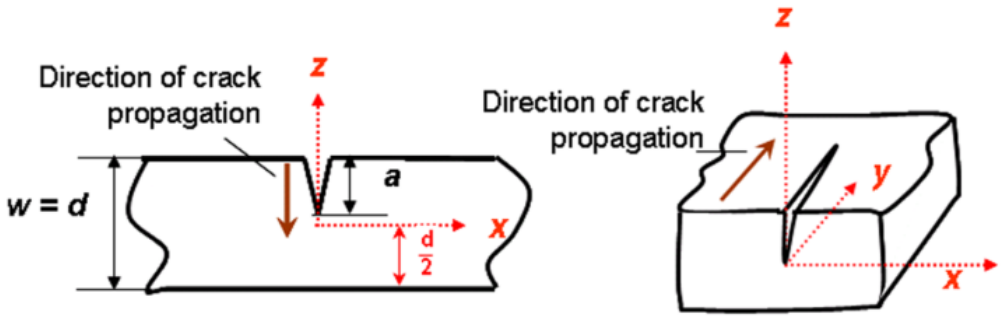

Figure 2.4. *(a): Plain strain crack (b): Crack channeling*

In the analysis of plane strain crack, J-integral evaluation developed by Rice[12, 13] was used as a fracture mechanics parameter to characterize the crack behavior. It is related to the energy release associated with crack growth and is a measure of the intensity of deformation at a notch or crack tip. It is defined in two dimensional as:

$$\mathrm{J} = \int_{\Gamma} \left(\mathrm{W} \cdot \mathrm{d}x_2 - T_i \cdot \frac{\partial u_i}{\partial x_1} \mathrm{ds} \right)$$

Where Γ is a contour surround the crack tip as shown in Figure 2.5(a); $W = \int \sigma_{ij} \mathrm{d}\varepsilon_{ij}$ is the strain energy density; $\mathrm{T_i} = \sigma_{\mathrm{ij}} \mathrm{n_j}$ is the surface traction vector, and u_i are the components of the displacement field.

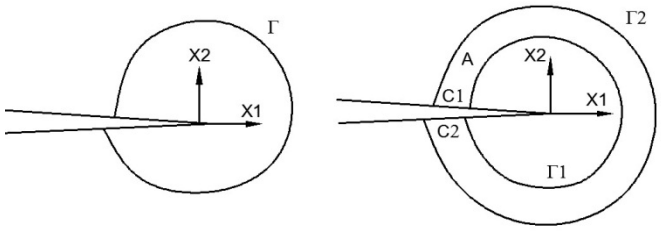

Figure 2.5. *(a): J integral contour (b): domain integral*

Shih[14] improved the J-integral from contour integral into domain integral as shown in Figure 2.5(b) for numerical evaluation and rewrite the equation using the divergence theorem in the form

$$J = -\int_A \left(W \cdot \frac{\partial q}{\partial x_i} - \sigma_{ij} \cdot \frac{\partial u_j}{\partial x_1} \cdot \frac{\partial q}{\partial x_i} \right) dA$$

where q is a sufficiently smooth weighting function within the region A enclosed by the contour $C_1\Gamma_1\Gamma_2C_2$ and has the value $q = 1$ on Γ_1 and $q = 0$ on Γ_2.

Abaqus provides a procedure for such domain evaluations of the J-integral. It uses all of the elements on the first layer outside the crack front as the first integral domain and provides output for more than one contour integral by adding a single layer of elements to the group of elements that were used to calculate the previous contour integral. Accuracy of results is not sensitive to the mesh types. It adds little to the cost of the analysis, and provided excellent accuracy, even with rather coarse meshes. Half of the workpiece was modeled in Abaqus and mesh used in this analysis is the rectangular one shown in Figure 2.6. J-integral values are independent of the couture at the out layers of elements.

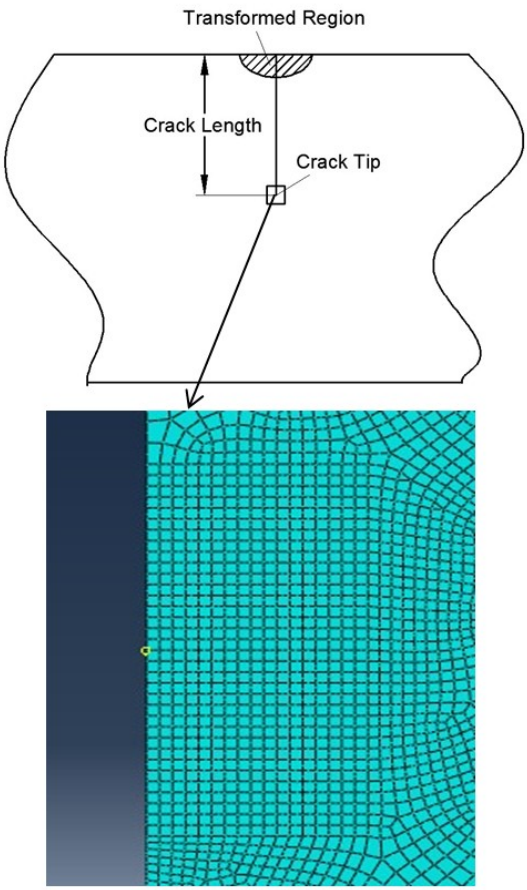

Figure 2.6. *Crack tip mesh configuration*

For the linear material response, J-integral can be related to the energy release rate as well as the stress intensity factors. Due to the extremely brittle of PCBN, the material response can be regarded as linear such that J-integral equals energy release rate value.

$$J = G(a') = \frac{K_I(a')^2}{E'}$$

where $G(a')$and $K_I(a')$ is the energy release rate and stress intensity factor for particular crack length a', $E' = E/(1-\nu^2)$ is the modulus for plane strain state. By assuming different crack length, the function of energy release rate verses crack length can be obtained for plane strain state crack.

The channeling of the edge crack is a three-dimensional problem. In our experiment, material separation along the cutting path due to phase transformation can be treated as steady-state crack propagation [15]. It is assumed that the crack propagated at a fixed depth and constant tip shape. Then the channeling process that the crack tip advances a unit distance is equal to removing a unit slice far ahead of the crack tip and attaching a unit slice with plane strain crack far behind the crack tip. The difference of energy stored in these two unit slice is the released energy U for crack propagates unit length. Apparently, it is just the released energy of the plane strain crack propagation and can be obtained by integration as

$$U = \int_0^a G(a')\,da'$$

And then, by definition, the energy release rate for the channeling crack is

$$G_{channeling} = \frac{U}{a} = \frac{1}{a}\int_0^a G(a')\,da'$$

2.4 Result and Discussion

2.4.1 Experimental results

For the first set of cutting experiments, fracture behavior were studied depend on the line energy (expressed in J/m). Observed fracture characteristics for the PCBN sample are plotted as a function of the line energy in Figure 4 for CO_2-LWJ machining. Three different fracture behaviors at different line energy were discovered. At the highest line energy (23.6kJ/m), a through cut was observed, indicating that the energy input was above the threshold value of through cutting. At the middle line energy (11.8kJ/m), a straight groove was found along the cutting path. Subsequently, the cracked sample could be completely separated with application of hand pressure with clean fracture surface and straight crack line.

The energy input at this level was at the threshold of through cutting over the thickness of this sample. At the lowest line energy (5.9kJ/m), only groove was observed on the sample surface. The grooved sample could not be separated on application of hand pressure after experiments.

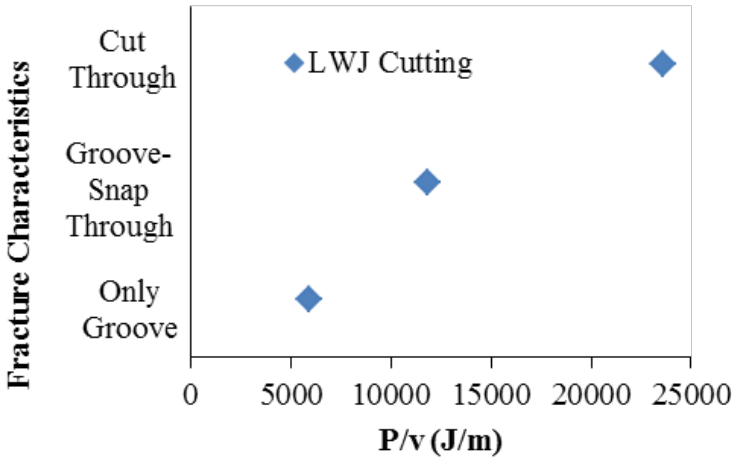

Figure 2.7. *Experimental results of fracture behavior*

SEM image of the through cut cross-section of LWJ machining at line energy of 23.6kJ/m (500 W laser power at 50 inches/min) is shown in Figure 2.8(a). Top view of scribing at line energy of 11.8kJ/m (500 W laser power at 100 inches/min) before snapping is shown in Figures 2.8(b). Top view of scribing at line energy of 5.9kJ/m (500 W laser power at 200 inches/min) is shown in Figures 2.8(c). In the through-cut case shown in Figure 2.8(a), two different regions can be clearly observed. The top region near the surface is the transformation zone that undergone phase transformation as well as material evaporation.

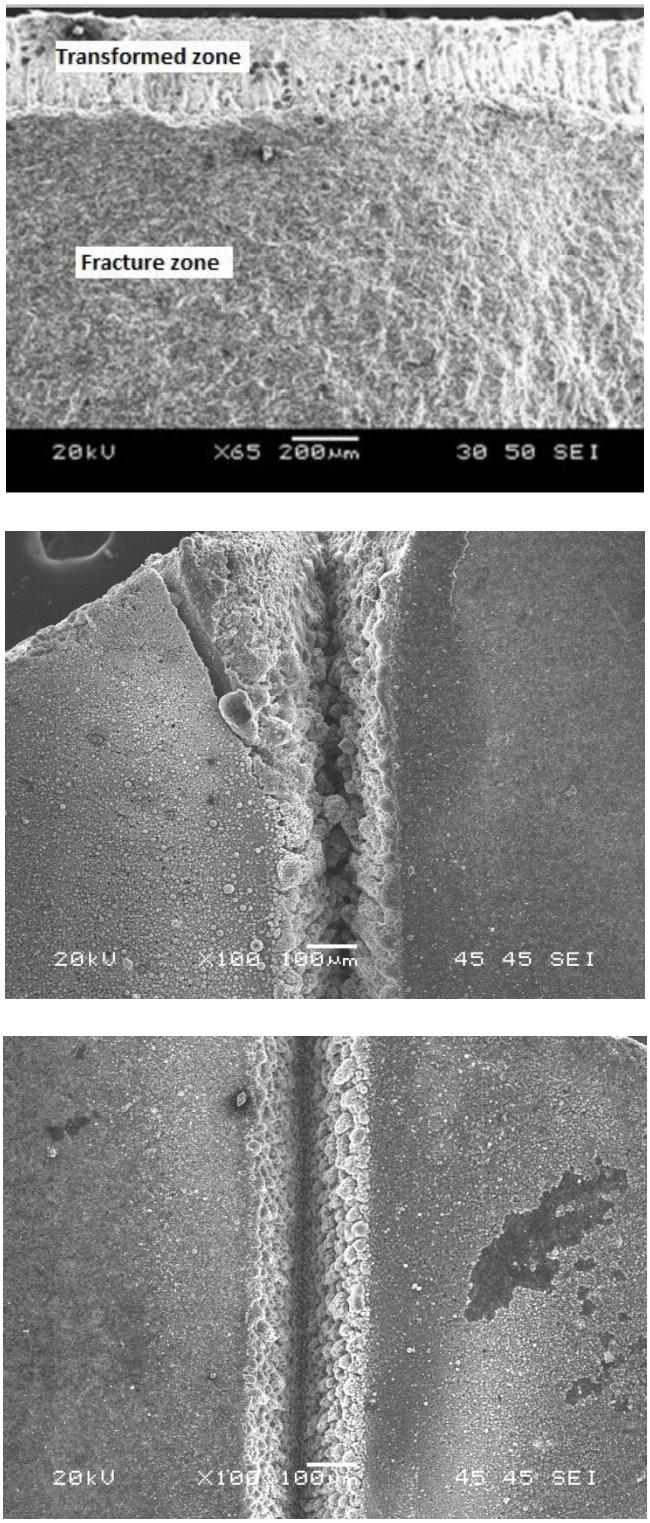

Figure 2.8. *SEM images of (a) Fracture cross section at line energy of 23.6kJ/m (b) Top view of scribing at line energy of 11.8kJ/m (c) Top view of scribing at line energy 5.9kJ/m*

The bottom region is the fracture zone resulted from propagation of cracks through the thickness due to transformation expansion. As shown in the image, the depth of transformation layer for through cutting is roughly 200 μm in average. In the scribing cases shown in Figure 2.8(b) and (c), recast layer along scribing line can be observed. Because of the rapid heat dissipation by water, narrow kerfs were produced and kerfs depth was found to be quite shallow. Furthermore, no visible lateral cracks were generated during LWJ cutting and sputtered particles below the recast layer were very insignificant.

Raman spectroscopy result of both the fracture zone and the transformed zone on the crack cross section is shown in Figure 2.9. The Raman spectrum of the as-received material is found to be similar to the fracture zone. Blue line in Figure 2.9 shows the spectrum of fracture region. Only cBN peak at 1302 cm-1[16] can be detected which reveals that there is no phase transformation happened here. However, on the transformed region, no cBN peak but two other phases was discovered. The peak around 1370 cm-1[17] proved that h-BN has been produced during laser heating and water quenching. The peak around 1580-1590 cm-1 was reported to be a graphite-like sp2-B-C-N atomic hybridization[18]. It can be result from the interaction between cBN and carbon impurities in the binder matrix. In both types of phase transformation, the volume of the original PCBN was expanded that helped in the material separation.

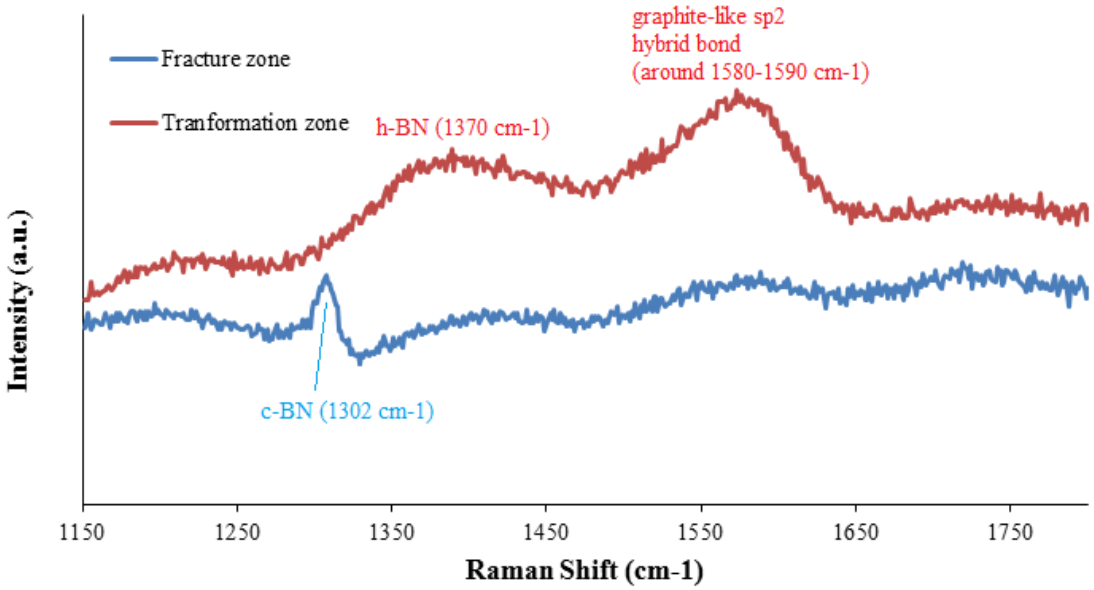

Figure 2.9. *Raman spectrum of transformed zone and fracture zone*

From the structure study and Raman result of machined sample, our understanding of the cutting mechanism is: (1) The sp3 bonded c-BN transformed into sp2-bonded BN phases between 1000 and 1800°C in the heat affected region; (2) These sp2-bonded phases melted and evaporated at temperature beyond 1000°C; (3) deposition of crystalline h-BN and BN whisker formation occurs resulted in the recast layer[10]. All these reactions mixed up with each other and happened instantaneously that lead to the crack propagation under stresses due to phase transformation expansion. This hypothesis is tested using the finite element model.

2.4.2 Validation of finite element model

Due to the accuracy limitation of FEM especially in describing functions with sharp change, we validated FEM solution with the exact solution in an axis-symmetric case of a

spherical region of dilatation in an finite elastic plate[19]. For axis-symmetric problem of an infinite body, Galerkin[20] introduced a stress function φ satisfying $\nabla^4\varphi = 0$ such that displacement components can be written as

$$u_r = -\frac{1}{2G}\frac{\partial^2\varphi}{\partial r\,\partial z}, \quad u_z = \frac{1}{2G}[2(1-\nu)\nabla^2\varphi - \frac{\partial^2\varphi}{\partial z^2}]$$

And stresses are

$$\sigma_r = \frac{\partial}{\partial z}\left[\nu\nabla^2\varphi - \frac{\partial^2\varphi}{\partial r^2}\right],$$

$$\sigma_\theta = \frac{\partial}{\partial z}\left[\nu\nabla^2\varphi - \frac{1}{r}\frac{\partial\varphi}{\partial r}\right],$$

$$\sigma_z = \frac{\partial}{\partial z}\left[(2-\nu)\nabla^2\varphi - \frac{\partial^2\varphi}{\partial z^2}\right],$$

$$\sigma_{r\theta} = \frac{\partial}{\partial z}\left[(1-\nu)\nabla^2\varphi - \frac{\partial^2\varphi}{\partial z^2}\right]$$

Where ∇^2 is Laplace operator, G is the shear modulus and ν is the poison ratio.

Yu and Sanday [19] introduced a method of integrating infinite virtual images to solve the boundary value problem of a finite plate of thickness h. The model can be described as a spherical region of dilatation located inside an elastic plate with boundary conditions of $\sigma(z = 0) = \sigma(z = h) = 0$. Compared with our model of a transformed region of expansion, the only difference is the shape and size of the region of dilatation. With proper integration, they found the stress function φ expressed in series in this case. By substituting φ in above equations, the final stress and displacement field can be obtained. We computed the analytical solution presented by Yu and Sanday for radial stress outside an expanding spherical cavity with radius of a. In addition, the finite element method was also utilized to

compute the same case. Comparison of FEM solution with analytical solution of reduced σ_r along z axis is presented in Figure 2.10.

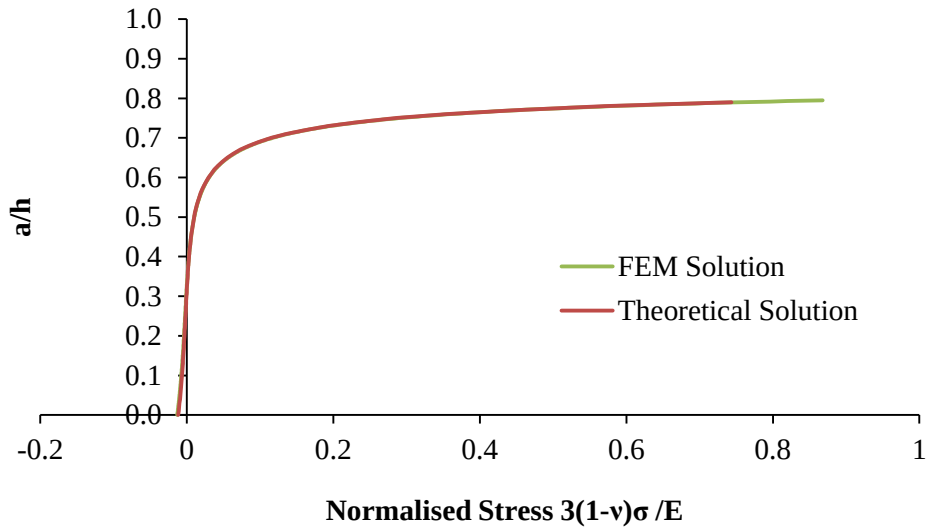

Figure 2.10. *Comparison of FEM with theoretical solution*

Mesh of the finite element model was refined till the computed stress became independent of the mesh size. The analytical and numerically computed stress distribution follow each other indicating that the finite element model can accurately determine the stresses induced due to expansion of the transformed zone.

2.4.3 Transformation strain and dimensions measurement results

In the second set of cutting experiments performed on thicker CBN samples, scribing was found in cuttings with all the parameters. It was observed from the sample side that the depth of the groove with the highest line energy of 37.8kJ/m (800 W laser power at 50 inches/min) was the deepest while the lowest line energy (9.4kJ/m) produced the shallowest

groove. The kerfs widths of the three scribing lines were found to be roughly the same size as the laser spot size (0.2 mm) from profilometer measurement results.

Surface profile of the workpiece was measured along lines normal to cutting path using optical profilometer for the three different line energy values. Measured profiles along 25 different lines were averaged to determine the surface deformation along the x direction. Average surface deformation as function of distance from the laser-cutting path is plotted for the three different line energy values in Figure 2.11. In order to determine the depth of transformation zone and effective transformation strain, numerical predictions of surface deformation were compared to measurements plotted in Figure 2.11.

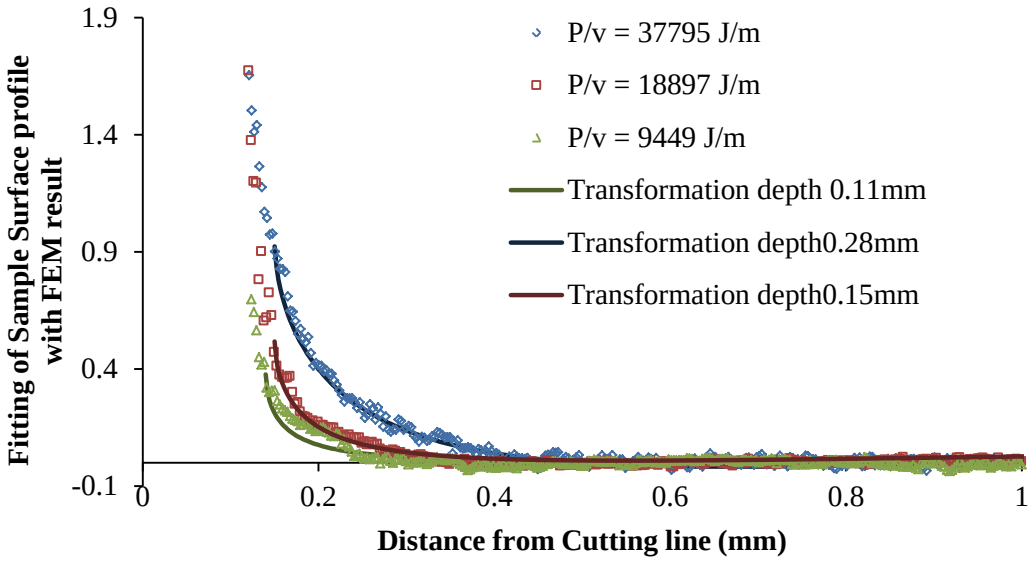

Figure 2.11. *Comparison of measured surface deformation and FEM based prediction*

The surface deformation was predicted assuming that the expansion strain in the transformed zone is constant and is independent of the laser line energy used during cutting. The effect of the line energy was approximated by assuming that the depth of the transformation zone increases with increasing line energy values. Based on the assumption

that all material heated above a threshold temperature is transformed, dimensions of the transformed material will be a linear function of heat input. Moreover, heat input is proportional to line energy. Therefore dimensions of transformation region should be roughly a linear function with line energy. In addition, transformation width was assumed to be constant due to the fact that the kerfs width was measured same of the three line energy values.

FEM calculations were performed for different values of expansion strain values and various dimensions of transformed zone were compared with the experimental measurement of surface deformation. FEM solutions that best describe the experimental results are shown in Figure 2.11. These solutions corresponded to an expansion stain of 0.013 and width of transformation zone of 0.15mm. Depths of transformation zone were 0.28mm, 0.15mm and 0.11mm for line energy values of 37.8kJ/m, 18.9kJ/m and 9.4kJ/m, respectively. The relationship between line energy and depth of transformation zone is plotted in Figure 2.12. The linear relation between the line energy value and depth of transformation indicates that the depth of transformation for different line energy values may be estimated using the linear relationship.

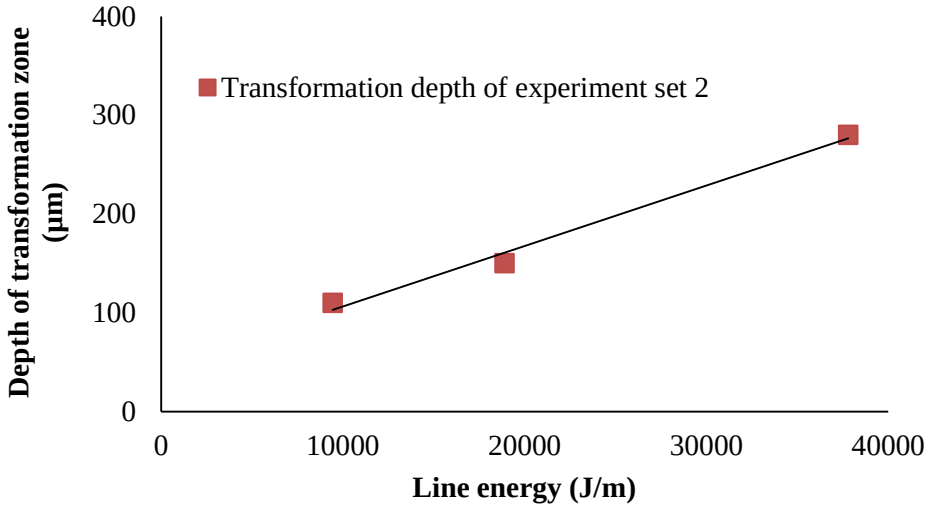

Figure 2.12. *Relationship between line energy with depth of transformation zone*

2.4.4 Fracture energy results and crack behavior prediction

The energy release rate in experiment set 1 for the plane strain edge cracks were calculated from J-integral evaluation for Mode I loading (in the x-z plane). The computed energy release rate for plane strain cracks representing the initial cut depth are plotted as a function of a/w (ratio of crack length to the thickness of material) for three different processing parameters in Figure 2.13. Energy release rates for channeling cracks representing crack propagation along the laser path are plotted for the same processing parameters in Figure 2.14. The three curves correspond to the line energy of first set of experiment, namely 23.6kJ /m, 11.8kJ /m, and 5.9kJ/m, respectively. It can be seen that initial cracks have different sizes in this three cases due to the compression stress inside the transformation region. Energy release rates G reach the highest for cracks that are approximately twice of the initial crack due to the large tensile stresses outside the transformation region induced from material expansion. It then decreases as the crack becomes longer due to the reduction

of tensile stress shown in Figure 2.13. Computed predictions of G are also compared to PCBN's critical energy release rate Gc in both Figure 2.13 and 2.14. Based on fracture mechanics theory, initial crack will propagate if the energy release rate exceeds the critical energy, otherwise crack will stop from growth. The average fracture toughness (critical value) of BZN7000 was reported to be 7.7-10 MPa$\sqrt{m}$ [21]. The calculated critical energy release rate was then 81-137 N/m. As shown in the Figure 2.13, energy release rate of 23.6kJ/m line energy for cracks up to 0.85 times the thickness is larger than the critical value, indicating that the plane strain crack at this cutting parameter can be created almost across the whole thickness. Energy release rate of 11.8kJ/m line energy lies right above the critical value, indicating the threshold energy input. Energy release rate of 5.9kJ/m is lower than the critical G which corresponds to the fact that no cracks other than groove has been generated. G for channeling crack also shows good agreement with experimental result (Figure 2.14). Channeling energy for 23.6kJ/m is higher than Gc representing the initial crack are expected to propagate along the laser path under the smooth driven force and create through-cut crack. Channeling energy for 11.8kJ/m locates on the critical range revealing the threshold cutting parameter. Channeling energy of 5.9J/m is lower than the critical value such that it is not able to be cut. The analytical result match well with experimental observations, therefore the analytical approach discussed above provide efficient estimation of phase transformation result, as well as the equilibrium depth of the channeling crack for each processing condition.

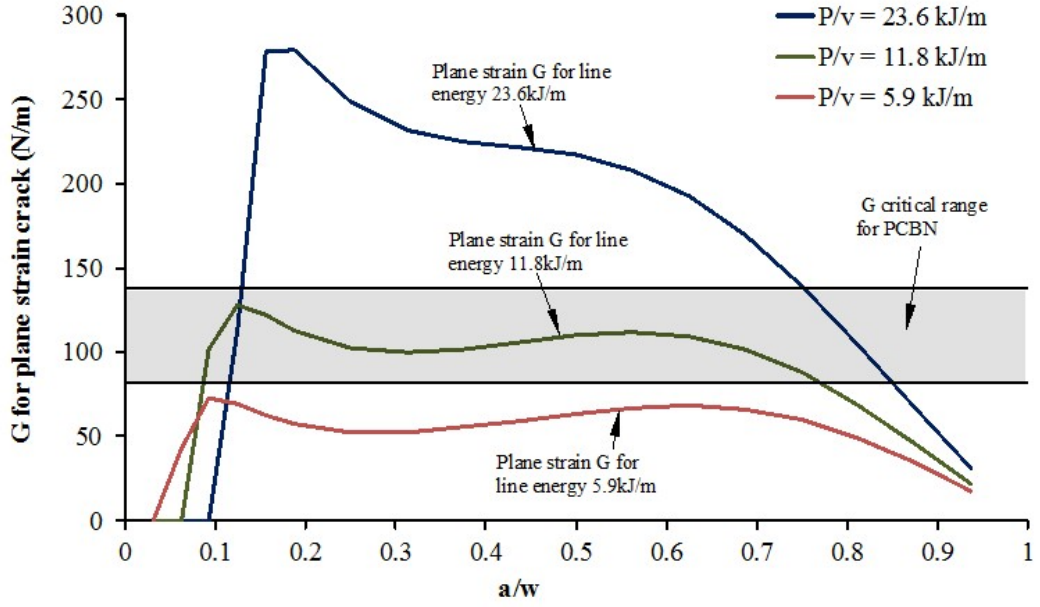

Figure 2.13. *Energy release rate for plane strain crack*

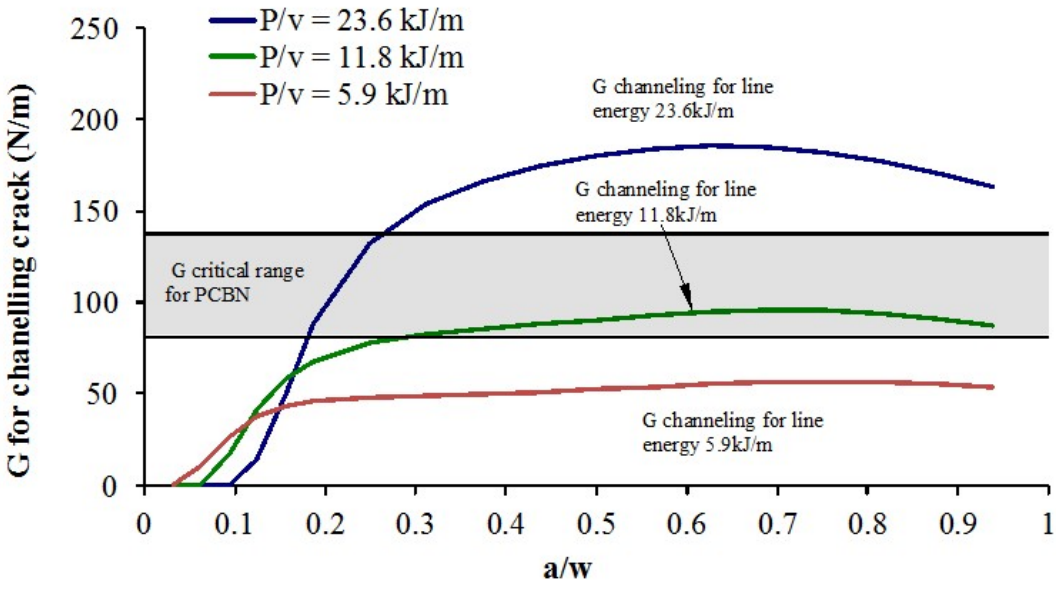

Figure 2.14. *Energy release rate for channeling crack*

2.5 Conclusion

Cutting experiments are conducted on two different thicknesses of PCBN blank inserts to achieve different purposes: study the effect of processing parameters on the fracture behaviors and obtain the size of phase transformed zone as well as associated expansion strain after laser heating. Three different fracture behavior observed from the first type of experiment indicate the threshold line energy for through cutting. Chemical testing results indicate that laser heated PCBN undergoes chemical phase transformation and material separation takes place due to propagation of cracks along the machining path. Based on the experimental observations and material properties, material separation is hypothesized to occur through crack propagation under the stress fields imposed due to the volumetric expansion associated with transformation of cBN to hBN and other sp2 phases. Measurement of transformation strain and dimensions of transformation region reveals a linear relationship between cutting line energy and transformation depth. Transformation stress with the obtained expansion strain and transformation volume was computed in FEM model. Energy release rate for channeling cracks was calculated and compared with experimental result. Good agreement between the analytical result and experimental observation demonstrated the feasibility of proposed mechanism for material separation through controlled crack propagation.

2.6 References

[1] R. H. Wentorf, "Synthesis of Cubic Form of Boron Nitride," Journal of Chemical Physics, vol. 34, pp. 809-&, 1961.

[2] P. B. Mirkarimi, K. F. McCarty, and D. L. Medlin, "Review of advances in cubic boron nitride film synthesis," Materials Science & Engineering R-Reports, vol. 21, pp. 47-100, Dec 15 1997.

[3] X. Ding, W. Y. H. Liew, and X. D. Liu, "Evaluation of machining performance of MMC with PCBN and PCD tools," Wear, vol. 259, pp. 1225-1234, 2005.

[4] H. Hidai and H. Tokura, "Hydrothermal-reaction-assisted laser machining of cubic boron nitride," Journal of the American Ceramic Society, vol. 89, pp. 1621-1623, May 2006.

[5] O. D. Sibailly, F. R. Wagner, L. Mayor, and B. Richerzhagen, "High precision laser processing of sensitive materials by Microjet," in Fourth International Symposium on Laser Precision Microfabrication, 2003, pp. 501-504.

[6] D. Kalyanasundaram, G. Shehata, C. Neumann, P. Shrotriya, and P. Molian, "Design and validation of a hybrid laser/water-jet machining system for brittle materials," Journal of Laser Applications, vol. 20, pp. 127-134, May 2008.

[7] D. Kalyanasundaram, P. Shrotriya, and P. Molian, "Obtaining a relationship between Process parameters and Fracture energy for CO2 Laser/Waterjet Machining of Ceramics," Journal of Engineering Materials and Technology, vol. 131, pp. 011005-10, 2009.

[8] C. Barnes, P. Shrotriya, and P. Molian, "Water-assisted laser thermal shock machining of alumina," International Journal of Machine Tools & Manufacture, vol. 47, pp. 1864-1874, Oct 2007.

[9] D. Kalyana-sundaram, J. Wille, P. Shrotriya, and P. Molian. (2008). CO2 Laser/Waterjet machining of Polycrystalline Cubic Boron Nitride.

[10] H. Sachdev, R. Haubner, H. Noth, and B. Lux, "Investigation of the cBN/h-BN phase transformation at normal pressure," Diamond and Related Materials, vol. 6, pp. 286-292, Mar 1997.

[11] J. Robertson, "Diamond-like amorphous carbon," Materials Science & Engineering R-Reports, vol. 37, pp. 129-281, May 24 2002.

[12] H. F. Bueckner, "A Novel Principle for Computation of Stress Intensity Factors," Zeitschrift Fur Angewandte Mathematik Und Mechanik, vol. 50, pp. 529-&, 1970.

[13] J. R. Rice, "A Path Independent Integral and Approximate Analysis of Strain Concentration by Notches and Cracks," Journal of Applied Mechanics, vol. 35, pp. 379-+, 1968.

[14] B. Moran and C. F. Shih, "A General Treatment of Crack Tip Contour Integrals," International Journal of Fracture, vol. 35, pp. 295-310, Dec 1987.

[15] S. Ho and Z. Suo, "Tunneling Cracks in Constrained Layers," Journal of Applied Mechanics-Transactions of the Asme, vol. 60, pp. 890-894, Dec 1993.

[16] H. Sachdev, "Influence of impurities on the morphology and Raman spectra of cubic boron nitride," Diamond and Related Materials, vol. 12, pp. 1275-1286, Aug 2003.

[17] L. Song, L. J. Ci, H. Lu, P. B. Sorokin, C. H. Jin, J. Ni, et al., "Large Scale Growth and Characterization of Atomic Hexagonal Boron Nitride Layers," Nano Letters, vol. 10, pp. 3209-3215, Aug 2010.

[18] M. A. Mannan, H. Noguchi, T. Kida, M. Nagano, N. Hirao, and Y. Baba, "Growth and characterization of stoichiometric BCN films on highly oriented pyrolytic graphite by radiofrequency plasma enhanced chemical vapor deposition," Thin Solid Films, vol. 518, pp. 4163-4169, May 31 2010.

[19] H. Y. Yu and S. C. Sanday, "Center of Dilatation and Thermal-Stresses in an Elastic Plate," Proceedings of the Royal Society of London Series a-Mathematical Physical and Engineering Sciences, vol. 438, pp. 103-112, Jul 8 1992.

[20] B. Galerkin, "Contribution to the general solution to the problem of the elasticity theory in the case of three dimensions.," Comptes Rendus Hebdomadaires Des Seances De L Academie Des Sciences, vol. 190, pp. 1047-1048, 1930.

[21] M. P. DEvelyn and K. Zgonc, "Elastic properties of polycrystalline cubic boron nitride and diamond by dynamic resonance measurements," Diamond and Related Materials, vol. 6, pp. 812-816, Apr 1997.

CHAPTER III

THE LASER/WATER-JET (LWJ) MACHINING OF DOUBLE-LAYER TUNGSTEN CARBIDE (WC) SUPPORTED POLYCRYSTALLINE CUBIC BORON NITRIDE (PCBN)

A paper prepared for *International Journal of Machine Tools and Manufacture*

Zhuoru Wu, Ammar Melaibari, Pal Molian and Pranav Shrotriya

Abstract

This paper presents a combined experimental and computational investigation of a novel thermochemical material removal mechanism for cutting of double-layer Tungsten Carbide (WC) supported Polycrystalline Cubic Boron Nitride (PCBN) substrates through controlled crack propagation. The CO2-LWJ machining system implemented a high power laser heating followed by low pressure waterjet quenching that achieved fracture initiation and propagation along the cutting path. Single-pass LWJ cutting of 1.6mm WC supported PCBN resulted in just a scribing on the sample surface instead of separation of the material. In order to achieve through-cut of the double-layer specimen, a new method of combining single-pass focused beam and multi-passes defocused beam was applied that successfully achieved complete cutting. Spalling cracks were observed in both focused and defocused cutting but the amount during defocused machining were apparently reduced compared with the focused cutting. Scanning electron microscopy (SEM) and Raman spectrometry were performed on the cut surfaces to identify the mechanism governing sample separation. The results suggest that during the localized laser heating and subsequent waterjet quenching, PCBN near the top surface underwent chemical transitions from sp3-bonded phase into sp2-bonded phases that induced volumetric expansion. Surface profile was experimentally

measured using profilometer and compared with analytical predictions in order to estimate the expansion strain and dimensions of transformation region. FEM model in ABAQUS was developed to determine the fracture behaviors associated with phase transformation. Fracture mechanics analysis of crack propagation is performed to validate the proposed governing mechanism. A possible method that inducing a wider and shallower transformation zone was suggested to reduce the spalling cracks and theoretical analysis was performed to explain the advantages and feasibility of this method.

KEYWORDS: Laser/waterjet machining (LWJ), defocused laser machining, PCBN, controlled fracture, phase transformation

3.1 Introduction

Cubic Boron Nitride (CBN) is the second hardest material on earth, and is a difficult-to-machine ceramic material due to its ultra-high hardness and good chemical and thermal stability. PCBN has been used in industry as a substitute for diamond due to the superior thermal and chemical stability. The advantages that PCBN does not react with ferrous metals and has a high resistance to oxidation[1] makes it ideal tool material for machining hard cast iron, high chrome alloy steels, high-strength nickel super alloys, powder metal alloys and metal matrix composites[2]. PCBN consists of fine crystals that are sintered under the conditions of high temperature and pressure with metallic(Co) or other binders. The common used binder phases including nickel[3], magnesium carbonate[4, 5] and ceramics (AlN and TiN). Similar to carbon, boron nitride exits both diamond-like sp3 bonded phases(cBN and wBN) and graphite-like sp2 phases (hBN and rBN) and transformation between these phases

would happen under high temperature or high pressure[6]. It was reported that the sp2-bonded structure occupies much more volume than sp3-bonded structure[7], therefore transformed material has an tendency to expand the original material.

PCBN tools are usually available in two forms: a solid compact or a composite with tungsten carbide substrate. While PCBN offers high wear resistance during machining, carbide substrates offer the required toughness as well as low cost making the composite tools an ideal choice for manufacturers. PCBN blanks in the thickness range 1.6 mm to 4.8 mm are available to making inserts in the form of rounds, squares, diamonds, and triangles designed to fit special usage in different industries.

Due to the extreme hardness, it is difficult to machine the PCBN tool blanks. During tool production, speed is an important criterion as cutting hard materials can be time-consuming. Typically speeds are on the order of few mm per minute. Many processes have been vigorously studied but none has the combination of speed, resolution and cost-effectiveness desired for industrial productivity. Current manufacturing methods for producing tool inserts in PCBN are diamond saw, wire-EDM and Nd:YAG laser cutting which are slow and less precise. Diamond saw is not acceptable due to rapid tool wear and slowness of the process. In addition, small kerfs are difficult to produce due to blade thickness. Electric discharge machining (EDM) [8, 9] and electric discharge grinding (EDG) [3, 10] of PCD are constrained by high machining cost, slowness and low efficiency. EDM cannot be used if the compact is not electrically conductive (example: PCBN with AlN binder). Conventional Nd:YAG laser cutting suffers from particle formation (due to vaporization) and thermal damages, conical kerfs and post processing becomes essential. Water jet-guided laser technology[11] - also known as Laser MicroJet® developed by

researchers in Swiss Federal Institute of Technology was an innovative technology that allows precise cutting of PCBN materials with smaller kerf and good surface finish. The concept of this technology is to focus a laser beam into a nozzle while passing through a pressurized water chamber. The free laminar waterjet is used as an optical waveguide to direct the Nd:YAG laser beam onto the sample. A Q-switched pulse laser (up to 300 W) of 532 nm wavelength and water pressure of 2-10 MPa was employed for the process. The waterjet permitted parallel beam transmission through the sample leading to taper-free and narrow kerf features. The tolerances are much smaller than those obtained with conventional laser and EDM processes. However the process suffers from very slow cutting speeds as it reports 120 passes with each pass at a speed of 25mm/s were needed to cut 1.6mm WC supported PCBN sample[11].

Given to the limitation of existing machining method of PCBN, a novel process of combining continuous wave CO2 laser and water-jet (LWJ) was developed by our group to improve the machining efficiency and quality of PCBN [4]. The CO2-LWJ machining system(schematically shown in Figure 1) implemented a high power laser heating followed by low pressure waterjet quenching that achieved fracture initiation and controlled propagation along the cutting path. Experiments on 1.6 mm thick solid PCBN (BZN 7000) supplied by Diamond Innovation Inc. showed that cutting speeds up to 42.3 mm/s could be readily achieved in single pass. Results have been recently published in MSEC/NAMRC41[12] Conference. The advantages of our CO2-LWJ over traditional Nd:YAG laser are finer kerf (crack width of few μm), parallel surfaces and minimal recast layer/HAZ and almost two orders of magnitude faster cutting speeds.

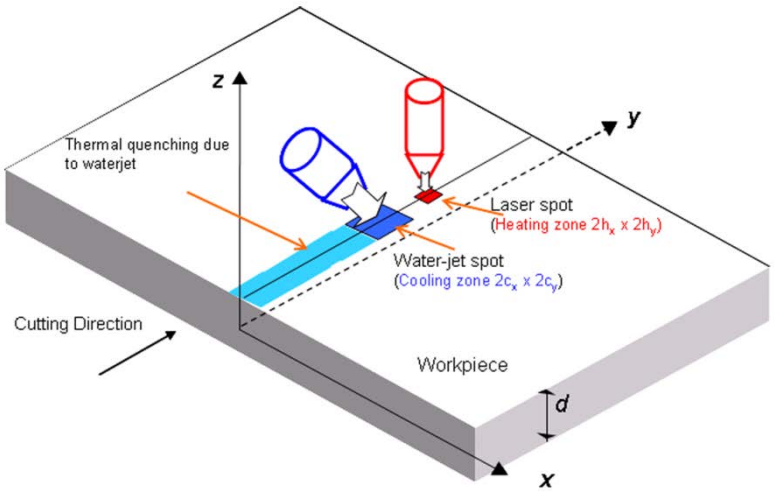

Figure 3.1. *Schematic representation of CO_2-LWJ machining setup*

Tsai and Chen[13] reported a laser cutting technique by controlled fracture used for the cutting of thick ceramic substrates by applying a focused Nd:YAG laser followed by a defocused CO2 laser. It successfully achieved the through cutting of thick alumina substrate along the moving path of the laser beams without a neat interface. Due to the observation of spalling crack and surface damages generated in LWJ cutting of WC supported PCBN, a similar technique combining single-pass focused beam and multi-passes defocused beam was applied aiming to reduce the uncontrolled lateral cracks. Results showed that the method was effective and apparently suppress the surface damages.

3.2 Experimental details

A continuous wave CO2 laser (Model 820 Spectra Physics) of 10.6 μm wavelength was used in all the experiments. Tool blank sample was mounted on a positioning workstation that controlled by a 2D CNC system. The beam from the laser was sent through

a focusing lens and irradiated on the sample surface. A 127 mm focal length lens was used to produce the focal spot diameter of 0.2 mm. A defocused spot with diameter larger than 0.2mm can be achieved through adjusting the distance between laser head and sample surface. The water jet trailed the laser beam on the sample surface with a spacing of 2 mm between them. A constant water pressure of 0.4Mpa (60 psi) was maintained in all the cutting experiments. Laser beam was surrounded by air with a pressure of 35kPa (5 psi) in order to prevent direct interaction of laser and water jet. During the experiments, laser beam was irradiated outside the sample, translated through and stopped out of the other side.

LWJ cutting experiment was conducted on a double-layer tungsten carbide (WC) supported PCBN blank, provided by Diamond Innovations, Inc. (Worthington, Ohio). The blank was 1.6mm thick wafer with 1mm thick PCBN sintered on 0.6 mm thick WC. The composition of PCBN was 50% with binder phase of 45% TiN and 5% AlN. Processing parameters was chosen to be 400 W of power and velocity of 42.32 mm/s (100 inch/min) of velocity based on previous cutting experience on solid PCBN sample. A new technique that combined single-pass focused beam and multiple passes defocused beam was also utilized in machining of this sample. The focused beam with spotsize of 0.2mm was first performed to create an initial groove, 4 passes of defocused beam with spotsize of 0.5mm were followed to make the stable crack propagates through the whole thickness. The power and speed used in this case was maintained at 400W and 100in/min.

In order to understand the mechanism and advantages of defocused LWJ cutting, another set of experiments was conducted on a PCBN sample with thickness of 4.8mm. The aim of this set of experiments was to replicate the laser effect produced on the thin sample for each pass without material separation. Same parameters of power and speed (400W and

100in/min) were implanted to replicate the crack conditions. Four cuttings were performed with different numbers of defocused passes carried out after the focus pass to study the progressive effect of the defocused beam. Number of defocused passes was 1, 2, 4 and 8 respectively for each cutting. Surface profiles around each scribing line were measured using an optical profilometer (Zygo NewView 7100). This instrument based on white light optical interference offers a noncontact, rapid method of characterizing 3D surface with a high resolution of 0.1 nm. Results were analyzed by statistical method to reduce variance. The measured surface profiles were compared with FEA model to obtain the size of phase transformed zone as well as the expansion strain associated with machining.

Scanning electron microscopy (SEM Model JEOL JSM-606LV at 20 kV) was used to inspect the cutting quality and provide critical dimensions as data input into the model. An optical microscope (Nikon) was used to measure the groove depth with a resolution of 1 micrometer. Raman spectroscopy (Renishaw-inVia Raman Microscopy) with Ar-ion laser at a wavelength of 532nm and power of 4mW was utilized to identify the phases present in the laser irradiated zone and fracture zone.

3.3 Numerical modeling

3.3.1 Finite element analysis for determination of transformation induced surface deformation and transformation strain

Our previous study on the focused single-pass cutting of solid PCBN showed a good correspondence between the experimental observations and FEA model[12]. The hypothesis is that laser irradiated zone of the PCBN workpiece undergoes a phase transformation that results in a volume expansion due to crystal structure transform. The volumetric change

initiates a local deformation around the cutting line and a tensile stress field underneath the region (Figure 3.2). This tensile stress induces the initial crack that propagated through the whole thickness and separated the material.

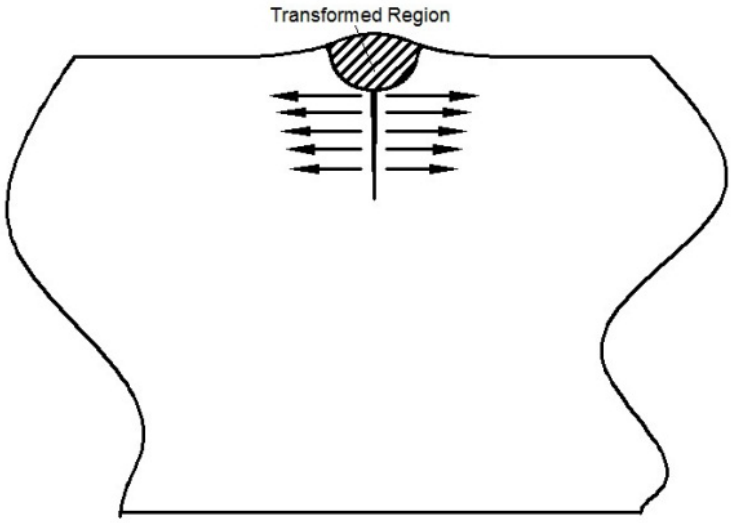

Figure 3.2. *Hypothesis for Crack propagation mechanism*

This paper will analyze the defocused LWJ cutting of the double-layer WC-PCBN specimen through the same mechanism. FEA models are developed to catch up the progressive effects of the defocused beam. Transformation zones undergoing uniform expansion was utilized to model the influence of material transformation along the cutting path. Material inside the transformation zone was applied the properties of hBN while material outside it was initial PCBN and WC. The detailed material properties are summarized in Table 1. 2-dimensional plane strain state was applied to the model since the laser cutting path was extremely long compared to the dimension of the transformation zone. Due to the symmetry, half of the workpiece was analyzed with fixed boundary condition on the axis of symmetry. Specific shapes and dimensions of transformation zone for each

defocused cutting line were determined based on the fitting of FEA computed surface deformation and experimental measurements of surface profile. Transformation strain kept as a constant value was also obtained from the best fitting result.

Table 3.1. *Material properties of PCBN, hBN and WC*

	Density (kg/m^3)	Thermal Conductivity (W/mK)	Specific Heat (J/kgK)	Poisson's Ratio	Young's Modulus (Gpa)	Thermal expansion coefficient	Fracture Toughness (Mpa√m)
PCBN	3450	200	900	0.15	710	5.6×10^{-6}	5-7.7
hBN	2010	360	600	0.2	70	2×10^{-6}	-
WC	15630	80	300	0.22	570	5×10^{-6}	12-19

3.3.2 Fracture mechanics analysis of cracks

Fracture mechanics analysis was performed to determine the crack propagation behavior for the defocused WC-PCBN cutting. The analysis follows same procedures as in previous study. Laser irradiation heats the surface and causes localized transformation and damage that results in crack nucleation and propagation. At the beginning of each cutting process, a crack is initiated at the edge of the specimen as the laser beam moved in. The crack extended towards center of plate and created an initial crack along the whole thickness. Plane strain analysis is proper to estimate the energy release rate of different crack length along the thickness direction. As the laser went further, the existing crack channeled along the laser path and achieved a through-cut that separated the specimen. This is the ideal status of the controlled fracture. However, some micro cracks might generate during the crack channeling and develop into uncontrolled spalling cracks that chipping off the materials

around cutting region. The three crack configurations are simplified and schematically shown in Figure 3.3.

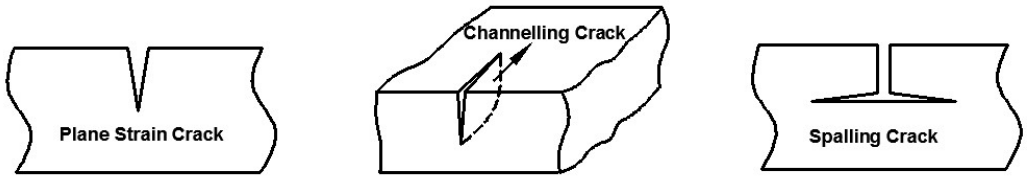

Figure 3.3. *(a): Plain strain crack (b): Crack channeling (c): Spalling crack*

In the 2D analysis of plane strain crack and spalling crack, J-integral evaluation was utilized as a fracture mechanics parameter to characterize the crack behavior. For the nearly linear material response as of PCBN and WC, J-integral equals energy release rate that:

$$G(a') = J = \int_{\Gamma} \left(W \cdot dx_2 - T_i \cdot \frac{\partial u_i}{\partial x_1} ds \right) \tag{3.1}$$

Where $G(a')$ is the energy release rate of a crack of length a', Γ is a contour surround the crack tip, $W = \int \sigma_{ij} d\varepsilon_{ij}$ is the strain energy density, $T_i = \sigma_{ij} n_j$ is the surface traction vector, and u_i are the components of the displacement field.

Numerical analysis was performed in commercial finite element analysis package ABAQUS (Simulia, Providence, RI). It provides a procedure to evaluate the J-integral of assigned number of layers of elements around the crack tip. Equilibrium will be reached at out layers of elements indicating that meshes were properly set. The simplified FEA model is shown in Figure 3.4. Vertical crack was assigned a length along the thickness direction. The crack length was increased from a small initial value below the transformation region to the rest of whole thickness such that the function of energy release rate verses crack length

throughout the thickness can be obtained. Spalling cracks were most found closed to the transformation region and was initiated from kinked micro cracks of the channeling crack. Therefore, initial spalling cracks were assumed to start from the vertical interface in a region just below the transformation zone. In this paper, only the initiation of spalling cracks was investigated while the propagation is not in the scope of discussion. In FEA model, the spalling cracks were assigned to a very small initial value at three locations below the transformation zone and an initial direction parallel to the sample surface was assumed. Energy release rates were calculated and compared with critical value of material properties. It is worthy to notice that the J-integral domain is not allowed to across the interface between inhomogeneous materials. To achieve the calculation of fracture energy around the interface, the crack lengths were chosen to be very close to the interface but crack tip contour lies in single PCBN or WC (Figure 3.5) without crossing the boundary. In such way, a narrow gap would appear in the plane strain energy curve but would not affect the integration in getting channeling fracture energy.

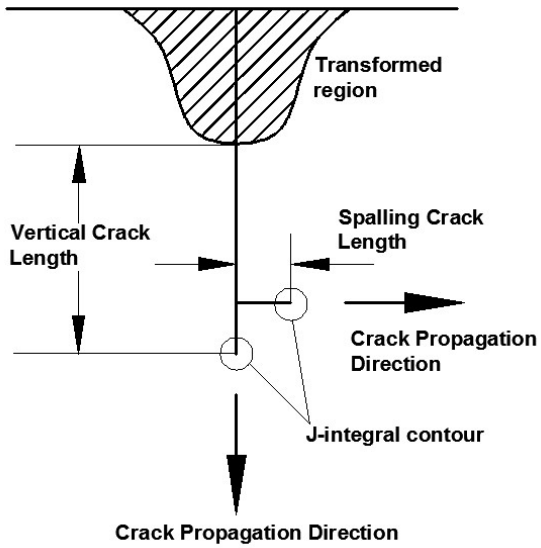

Figure 3.4. *FEA model for J-integral evaluation for both vertical and spalling cracks*

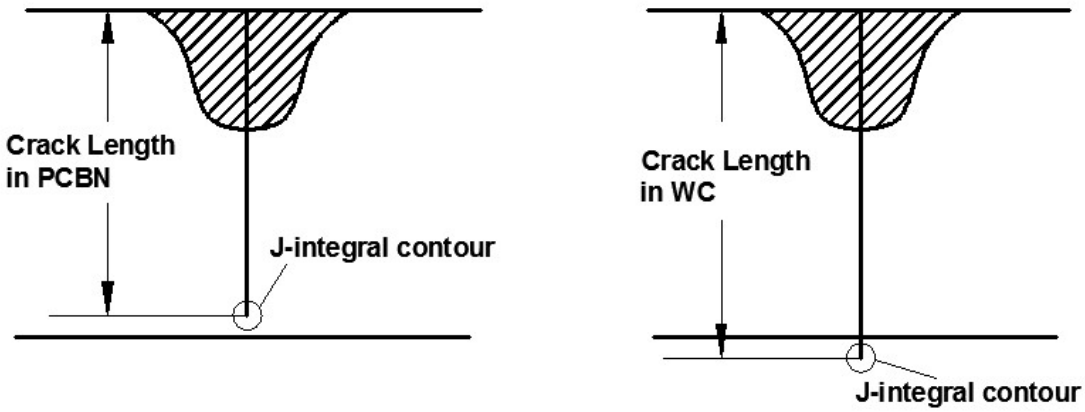

Figure 3.5. *J-integral contour without crossing material interface*

The channeling of the vertical plane strain crack is the three-dimensional process that resulted in separation of the specimen. Base on the assumption that the crack propagated at a fixed depth and constant tip shape, the energy required for this crack configuration is determined by equation[14]

$$G_{channeling} = \frac{1}{a}\int_0^a G(a')\,da' \tag{3.2}$$

Where $G(a')$ is the fracture energy for plane strain cracks of various depth.

Computed energy release rate was compared to the weighted channeling energy release rate of materials to predict the fracture behavior based on fracture mechanics theory. For a unit advance of the channeling crack, the required energy is balanced by the energy needed to create crack surfaces as[15]

$$G_{critical} = h\Gamma_{PCBN} + (a-h)\Gamma_{WC} \tag{3.3}$$

Where Γ_{PCBN} and Γ_{WC} are critical fracture energies for PCBN layer and WC layer and h is the thickness of PCBN layer.

3.4 Result and discussion

3.4.1 LWJ cutting results

In the single-pass cutting of WC supported PCBN with designed parameters (100in/min, 400W), only a superficial scribing with no material separation was observed (Figure 3.6(A)). Increasing energy input or reduce cutting speed or repeating focused cutting will cause severe damages of the specimen (Figure 3.6(B)). Due to the failure attempts of cutting with focused beam, the defocused beam was introduced to achieve a through-cut. The multiple-passes defocused beam after scribing of focused beam was performed successfully and achieved through-cut of this double-layer sample without much surface damage (Figure 3.6(C)). However, sometimes spalling cracks can still be observed but apparently less compared to the focused cutting (Figure 3.6(D)).

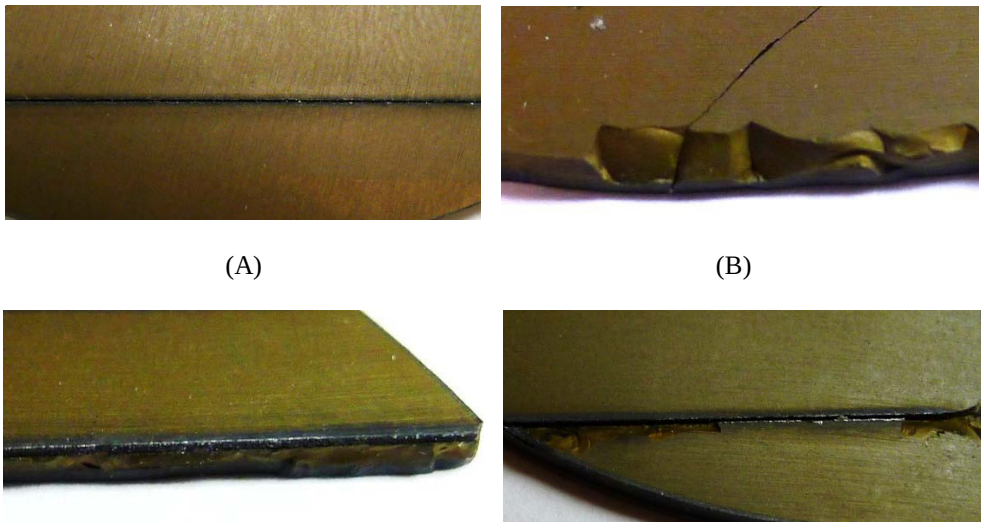

(A) (B)

(C) (D)

Figure 3.6. *(A) Superficial scribing: single-pass cutting of PCBN/WC (B) Severe damage: high energy input for single-pass cutting (C) Through-cut: multi-passes defocused cutting (D) Less spalling cracks: multi-passes defocused cutting*

SEM micrographs were taken for study of small features after multiple passes defocused LWJ machining. The through-cut cross-section of WC supported PCBN sample is shown in Figure 3.7(A). Three distinct different parts are marked as transformation zone, fracture zone and WC fracture zone. The one near top surface is the transformation region that undergone chemical transformation as well as melting. Below that is the fracture region formed due to propagation of cracks through the thickness. A third region of fractured WC can be observed at the bottom of this image. Based on the scale shown, the transformation depth for the WC-PCBN sample are roughly 400μm. Compared to 200μm of solid PCBN obtained in previous research, the multiple defocused laser beam transformed material in a deeper region twice of the single-pass focused beam. The obtained values are important input data of the FEA model such that the depth of the semi-ellipse transformation region can be determined. Figure 3.7(B) shows the chipping-off of the transformation region by multiple defocused cutting. This phenomenon was resulted from structure change of transformed material and development of microcracks around the transformation region during laser cutting. The interface between two layers of different materials was another vulnerable location that defects or microcracks might exist in the original blanks. Figure 3.7(C) shows the spalling cracks started from the material interface that lead to PCBN layer peeling off from the WC layer. The severe damage not only caused a waste of material but brought inconvenience to the post processing of the specimen, which need to be eliminated in some way.

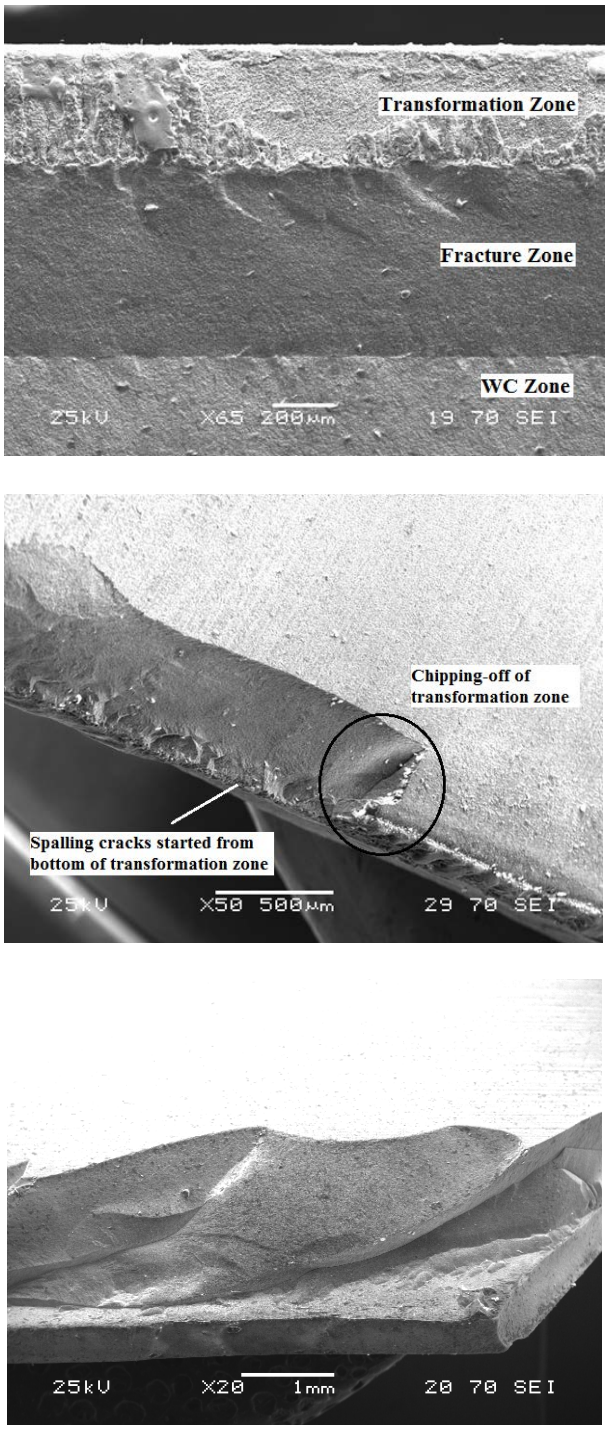

Figure 3.7. *(A) Cross-section of WC-PCBN sample after 4 times of defocused machining (B) Chipping-off of the transformation region (C) Spalling cracks at the interface between layers*

3.4.2 Raman spectroscopy result

Raman spectroscopy was carried out on both fracture region and transformation region. Figure 3.8 shows the comparison result between them. In the fracture region, only cBN peak at 1059cm-1 and 1302 cm-1[16] can be detected which reveals that the fracture region was original PCBN material. In the transformed region, only hBN peak at 1370cm-1was discovered [17] proving that phase transformation happened and produced hBN from original PCBN during laser heating and water quenching. The Raman result validated the hypothesis that the laser irradiated zone of the PCBN workpiece undergoes a phase transformation that results in a volume expansion and helped in the material separation.

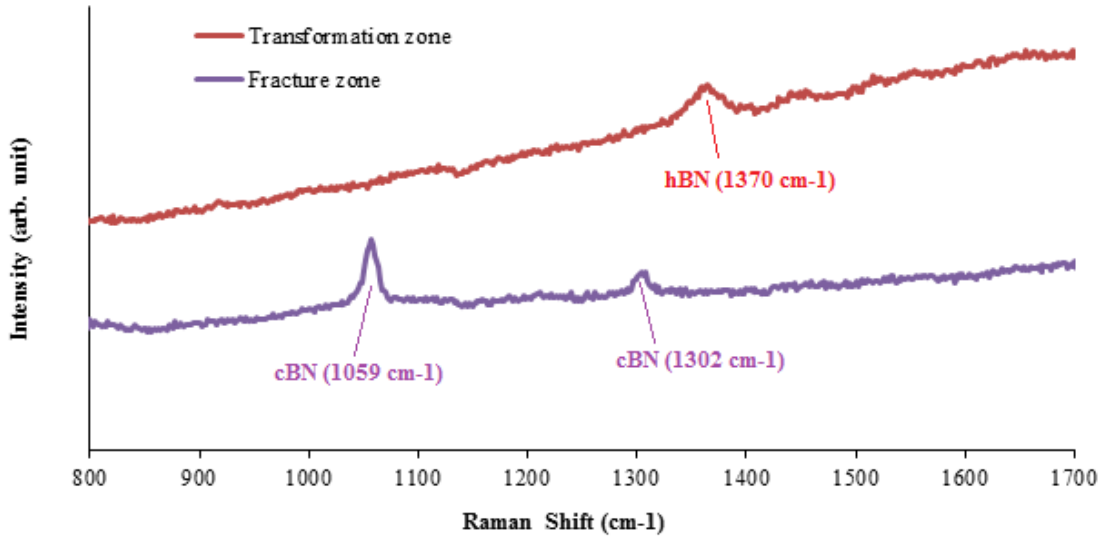

Figure 3.8. *Raman spectrum of transformed zone and fracture zone*

3.4.3 Surface profile measurement and comparison with FEA analytical result

In the testing experiments performed on the thicker PCBN samples, only scribing were made for the four cases with different numbers of defocused passes after the first

focused pass. Surface profile was measured along each scribing line and the average value determined their surface deformation. Averaged surface profile as a function of distance from the center of cutting path is plotted for the four cases with 1, 2, 4 and 8 defocused passes in Figure 3.9. The result shows the progressive effect of the 0.5mm defocused beam. One pass case has the least deformation indicating that only small amount of material was transformed. As the number of pass increasing, more material has been transformed resulting in the higher and wider breakout of material. Profiles of four passes and eight passes are nearly overlapping revealing that material has already been fully transformed with four defocused passes. The width of the breakout zone (0.3mm in half) corresponds well with the diameter of defocus beam (0.25mm in half). The kerfs widths of the four scribing lines were found to be roughly the same(0.11mm in half) and match the focused laser spot size (0.1 mm in half) from this profilometer measurement results.

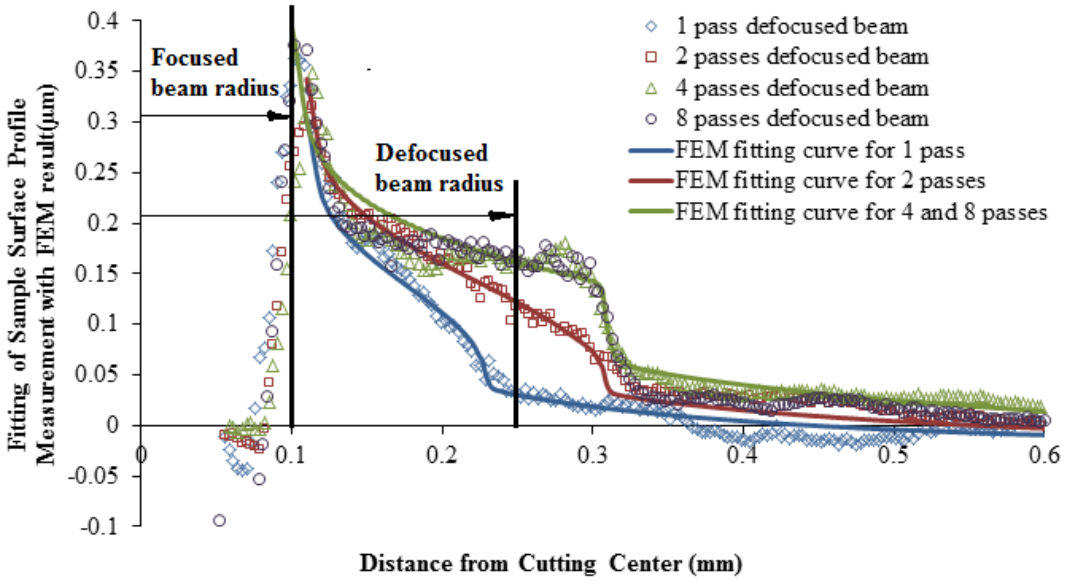

Figure 3.9. *Surface profile the four lines with 1, 2, 4 and 8 defocused passes and comparison of the measured data with FEM based prediction*

Based on the surface profile measurements, our understanding of the development of the transformed region for multiple defocused laser passes is shown in Figure 3.10. At first, the focused beam created a transformed region slightly larger than the laser spotsize and an initial groove was generated at the central part of the region. After that, defocused passes applied on the same location transformed materials in both a wider and a deeper region. Groove depth also increased due to the laser effect. Stresses induced by the expansion of the vertical region helped the crack to propagate through thickness; stresses induced by the surface expansion region helped to suppress the spalling crack.

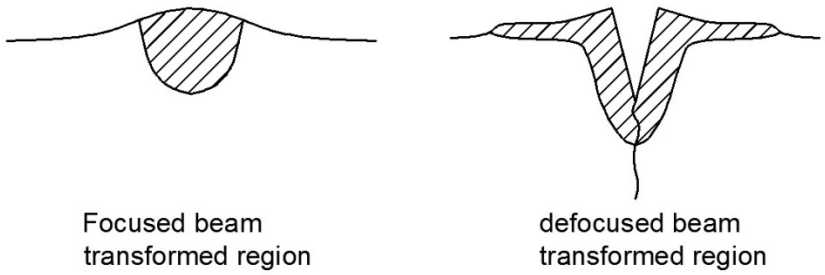

Figure 3.10. *Development of the transformed region for multiple defocused laser passes*

The FEA computed results are also plotted in Figure 3.9 for determination of the shapes and dimensions of the transformed zones with a constant expansion strain value. Cross-sections of the overall transformation zone were composed of a deep and narrow zone induced in the vertical direction as well as a wide and shallow zone induced near surface by the defocused beam. The transformation zone along depth direction was modeled as semi-ellipse in order to approximate the influence of the laser with a Gaussian intensity. The width of transformation zone was chosen to be 0.22mm in all the four cases that was slightly larger than the focused laser spotsize of 0.2mm that can well fit the surface profile. The depth of the

transformation zone was obtained from cutting interface of SEM images (200μm for single-pass focused cutting and 400μm for 4-passes defocused cutting). The transformation zones near surface induced by the defocused beam were chosen to be different shapes to catch up the surface profile measurements of the 4 cutting lines. The groove was simplified to a triangle subtracted from workpiece with depth measured from microscope. Groove width was kept as a constant value of 0.2mm based on the similar surface profile measurement of the four conditions. The overall cross-section of the transformation zone in FEA model was approximated by assuming shapes of transformation zone developed as shown in Figure 3.11. The specific shape and dimensions applied in this model is summarized in Table 3.2.The fitting result in Figure 3.9 indicated that the chosen shapes were capable to reflect the progressive effect of the defocused cutting passes. All these solutions corresponded to a constant expansion strain of 0.008.

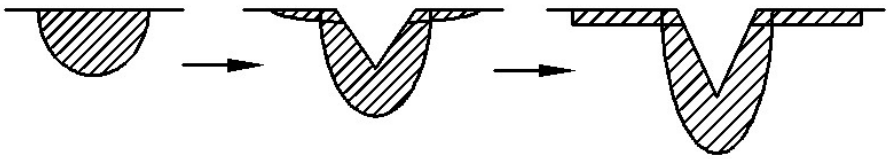

Figure 3.11. *Simplification of the transformed region for multiple defocused laser passes in FEA model*

Table 3.2. *Shape and dimensions of transformation zone near surface*

# of defocused passes	Transition depth	Groove depth	Shape of transformation zone near surface	Dimensions of transformation zone near surface
0	200um	0	-	-
1	250um	150um	ellipse	Depth: 5um, width:220um in half
2	300um	160um	ellipse	Depth: 5um, width:300um in half
4&8	400um	175um	rectangle	Depth: 5um, width:300um in half

3.4.4 Energy release rate calculation of vertical cracks

The energy release rate was computed for two cases: the single-pass scribing of WC supported PCBN and the multiple defocused cutting of WC supported PCBN that achieved through-cut. Fracture energy of plane strain cracks in thickness direction was calculated from J-integral evaluation for phase transformation induced loading. Channeling energy release rate obtained by equation (3.2) was the accumulation of plane strain cracks scaled by crack length. The computed channeling energy release rate for both single-pass focused cutting and 4-times defocused cutting are plotted in Figure 3.12 as a function of a/w (ratio of crack length to the thickness of material) corresponding to cutting parameters of 100in/min and 400W. The dimensions of transformation zone of single-pass cutting were obtained from the data of solid PCBN specimen machined with same cutting conditions. Dimensions due to defocused cutting were applied to the data of 4&8 passes presented in Table 3.2. Computed energy release rate was also compared to the weighted energy release rate obtained from equation (3.3) for the double-layer specimen . The fracture energy of WC reported to be

240N/m-602N/m[18] was much higher than the PCBN reported as 81N/m-137N/m in literature[19].

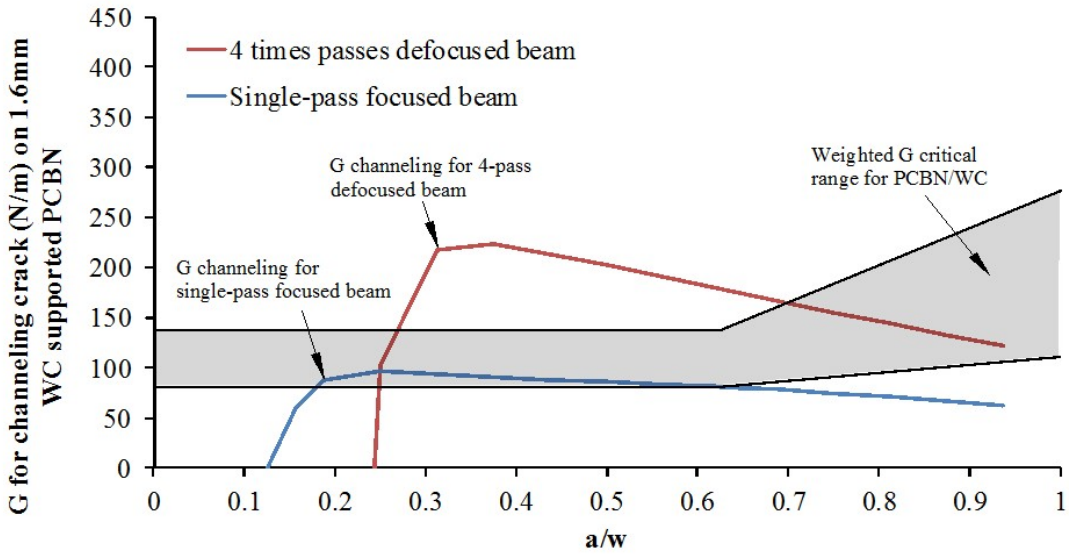

Figure 3.12. *Energy release rate for channeling crack machined with single-pass focused beam and 4 times defocused beam*

Based on fracture mechanics theory, initial crack will propagate if the energy release rate exceeds the critical fracture energy of material, otherwise crack will stop from growth. As shown in Figure 3.12, magnitudes of energy release rates for the single-pass focused beam was lower than most of the critical range of PCBN and WC that was not able to drive the initial crack. While the energy release rates for 4 times defocused beam improved more than twice that capable to drive the crack to 0.7-1 times of the whole thickness. Besides the increase of fracture energy, defocused LWJ machining also applied thermal shock to the whole specimen leading to degradation of fracture toughness of tungsten carbide. Dongbin Han and John Mecholsky[20] reported that the toughness of tungsten carbide decreased 20%

in 3 times of thermal shock with temperature gradient of 400ºC(shown in Figure 3.13). The similar situation happened in the multiple defocused LWJ machining that lead to the reduction of critical energy release rate of tungsten carbide that also helped the crack to propagate through.

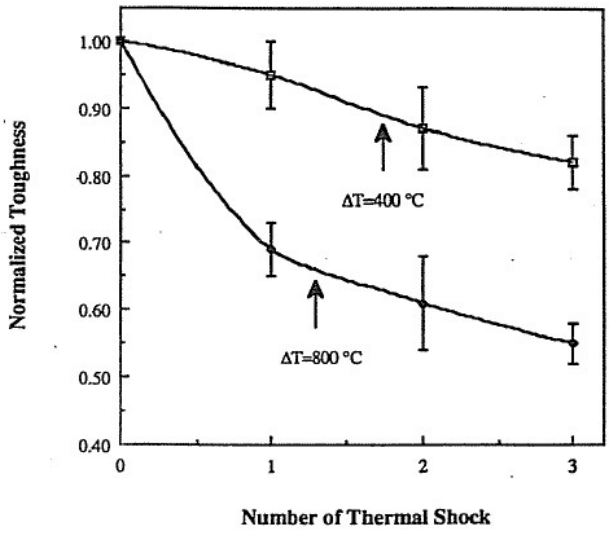

Figure 3.13. *Degradation of fracture toughness of WC due to thermal shock[20]*

3.4.5 Fracture energy calculation of spalling cracks and a possible solution to reduce them

The spalling cracks were developed from some micro cracks generated during channeling crack propagation. In this paper, only the initiation of spalling cracks was investigated and discussed while the propagation is not in the scope of discussion. Experimental observation suggested that two vulnerable locations were most probable for initiation of spalling cracks: the region just below the transformation zone and the interface between two layers. The interface crack might come from the defects in the original tool blank during sintering procedure; therefore it is not going to be discussed in this paper.

The spalling cracks near transformation zone were investigated for three cases: the single-pass focused cutting, multi-passes defocused cutting and a designed case aiming to reduce spalling cracks. Based on the experimental observation that spalling cracks during defocused LWJ machining were less than the focused cutting, we put forward a hypothesis that the transformation zone induced in a wider region will help to suppress the lateral spalling cracks. To test this assumption, a FEA model with a wider but shallower region of transformation zone was developed to compare with the actual cases. The dimensions of the region was designed to make sure that the magnitude of fracture energy for channeling crack was above the critical value so that the crack can propagate through. A case design that satisfied the through-cut condition is the transformation zone of an ellipse shape of 0.6mm in width and 0.25mm in depth as shown in Figure 3.14(C). For the single-pass focused cutting, the transformation depth required to cut through the whole thickness would be much deeper than that of the defocused beam (400μm) as the fracture toughness of WC was maintained the original value. FEA analysis followed the same procedure as described above determined that 600μm deep zone was required to achieve a through-cut for focused single-pass cutting. The specific dimensions of transformation zone for these three cases are represented in Figure 3.14.

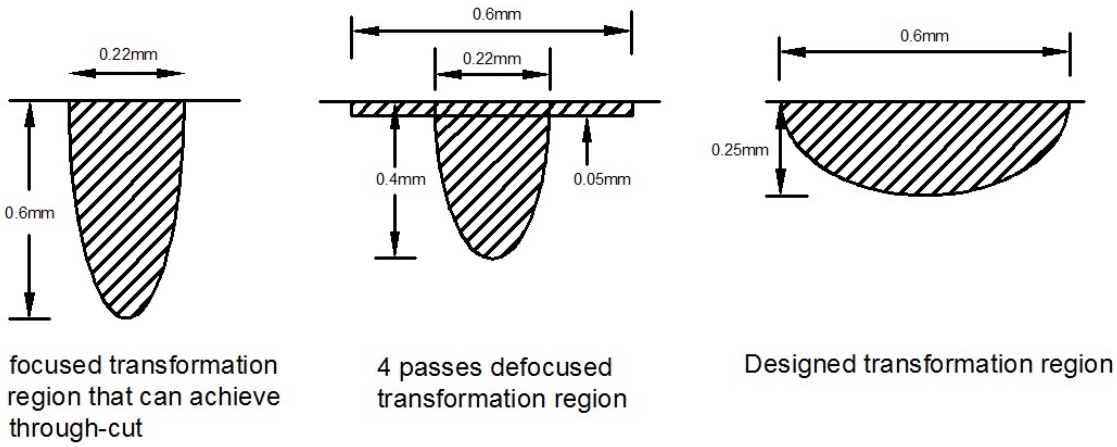

Figure 3.14. *(A)Focused cutting transformation zone (B) Defocusd cutting transformation zone (C) Designed transformation zone*

In in all the three cases, lateral cracks were assigned to a very small initial value of 0.016mm (a/w =0.01) and an initial direction parallel to the sample surface at three locations: 0.016mm(0.01w), 0.048mm(0.03w) and 0.08mm(0.05w) below the transformation zone. Figure 3.15 shows the energy release rate of spalling cracks for the three cases. The single-pass focused beam induced the largest fracture energy that was most possible to drive the initial crack propagate. The designed rectangle transformation zone induced compressive stress field under it that intent to close the crack and resulted in the zero fracture energy. In all the three cases, energy release rate decreased as the initial crack location getting far away from the transformation zone. Therefore the region around it was the most probable location for inducing of spalling cracks. The analytical results correspond well with the observation that the focused cutting induced more spalling cracks than the defocused cutting. In addition, a wider and shallower transformation shape is feasible to reduce or even eliminate the spalling cracks.

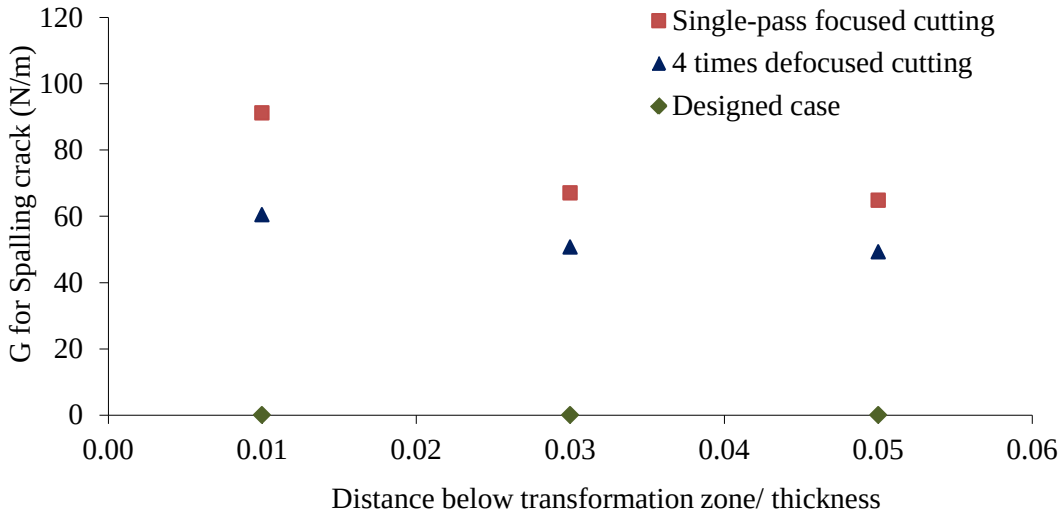

Figure 3.15. *Energy release rate of 0.01w spalling cracks at 0.01w, 0.03w and 0.05w below transformation zone*

3.5 Conclusion

LWJ Cutting experiments are conducted on 1.6mm tungsten carbide supported PCBN with process parameters of 100in/min and 400W. The specimen resulted in just a scribing on the sample surface instead of separation of the material. A new method of performing multi-passes defocused beam after the scribing of single-pass focused beam was applied on the double-layer sample that successfully achieved complete cutting. In order to understand the function of the defocused beam, a set of experiments was performed on a 4.8mm thick PCBN piece with 1, 2, 4 and 8 defocused passes after the scribing of focused beam aiming at duplicate the cutting effect during defocused machining without material separation. Spalling cracks happened sometimes and the defocused machining can apparently suppress uncontrolled lateral cracks compared with the focused one.

Based on the experimental observations and previous Raman testing result, material separation is hypothesized to occur through crack propagation under the stress fields imposed by the volumetric expansion associated with phase transformation of PCBN. FEA model with a transformation zone near top surface undergoing uniform expansion was utilized to model the influence of material transformation along the cutting path. Transformation depth was determined from SEM image of cut interface to be 200μm for single-pass cutting and 400 μm for multi-passes defocused cutting. Surface profile of the 4.8mm PCBN for study of defocused beam was measured using profilometer and compared with FEA model to estimate the expansion strain and dimensions and shapes of transformation region. The best fitting expansion strain was found to be 0.08. Energy release rates of crack propagation were calculated in FEA model. The degradation of fracture toughness of WC for 20% due to repeated thermal shock was introduced to explain the through-cut of WC supported PCBN. Initiation of spalling crack was also studied in this paper. The energy release rate of spalling crack for three cases were calculated: the single-pass focused cutting, multi-passes defocused cutting and a designed case aiming to reduce lateral cracks. Results indicate that a wider and shallower transformation zone will be benefit to reduce the spalling cracks.

3.6 References

[1] P. B. Mirkarimi, K. F. McCarty, and D. L. Medlin, "Review of advances in cubic boron nitride film synthesis," Materials Science & Engineering R-Reports, vol. 21, pp. 47-100, Dec 15 1997.

[2] X. Ding, W. Y. H. Liew, and X. D. Liu, "Evaluation of machining performance of MMC with PCBN and PCD tools," Wear, vol. 259, pp. 1225-1234, 2005.

[3] X. L. Liu, Y. F. Li, F. G. Yan, Y. Wang, J. S. Hu, and Y. J. Wang, "Study on precision grinding technique of PCD tool's cutting edge," in Advances in Grinding and Abrasive Technology Xiii. vol. 304-305, ed, 2006, pp. 186-190.

[4] M. Akaishi and S. Yamaoka, "Physical and chemical properties of the heat resistant diamond compacts from diamond-magnesium carbonate system," Materials Science and Engineering a-Structural Materials Properties Microstructure and Processing, vol. 209, pp. 54-59, May 1996.

[5] T. Irifune, A. Kurio, S. Sakamoto, T. Inoue, and H. Sumiya, "Materials - Ultrahard polycrystalline diamond from graphite," Nature, vol. 421, pp. 599-600, 2003.

[6] H. Sachdev, R. Haubner, H. Noth, and B. Lux, "Investigation of the cBN/h-BN phase transformation at normal pressure," Diamond and Related Materials, vol. 6, pp. 286-292, Mar 1997.

[7] J. Robertson, "Diamond-like amorphous carbon," Materials Science & Engineering R-Reports, vol. 37, pp. 129-281, May 24 2002.

[8] Y. H. Liu, Y. F. Guo, and J. C. Liu, "Electric discharge milling of polycrystalline diamond," Proceedings of the Institution of Mechanical Engineers Part B-Journal of Engineering Manufacture, vol. 211, pp. 643-647, 1997.

[9] P. L. Tso and Y. G. Liu, "Study on PCD machining," International Journal of Machine Tools & Manufacture, vol. 42, pp. 331-334, Feb 2002.

[10] J. Y. Pei, C. N. Guo, and D. J. Hu, "Electrical discharge grinding of polycrystalline diamond," in Advances in Materials Manufacturing Science and Technology. vol. 471-472, ed, 2004, pp. 457-461.

[11] A. Pauchard, M. D. Marco, B. Carron, G. Suruceanu, B. Richerzhagen, A. Brulé, et al., "Recent Developments in the Cutting of Ultra Hard Materials Using Water Jet-Guided Laser Technology," presented at the ALAC, 2008.

[12] Z. Wu, A. A. Melaibari, P. Molian, and P. Shrotriya, "The Mechanism Governing Cutting of Polycrystalline Cubic Boron Nitride (PCBN) with Transformation Induced Fracture," presented at the MSEC/NAMRC 41, Madison, WI, 2013.

[13] C. H. Tsai and H. W. Chen, "Laser cutting of thick ceramic substrates by controlled fracture technique," Journal of Materials Processing Technology, vol. 136, pp. 166-173, May 10 2003.

[14] S. Ho and Z. Suo, "Tunneling Cracks in Constrained Layers," Journal of Applied Mechanics-Transactions of the Asme, vol. 60, pp. 890-894, Dec 1993.

[15] T. Ye, Z. Suo, and A. G. Evans, "Thin-Film Cracking and the Roles of Substrate and Interface," International Journal of Solids and Structures, vol. 29, pp. 2639-2648, 1992.

[16] H. Sachdev, "Influence of impurities on the morphology and Raman spectra of cubic boron nitride," Diamond and Related Materials, vol. 12, pp. 1275-1286, Aug 2003.

[17] L. Song, L. J. Ci, H. Lu, P. B. Sorokin, C. H. Jin, J. Ni, et al., "Large Scale Growth and Characterization of Atomic Hexagonal Boron Nitride Layers," Nano Letters, vol. 10, pp. 3209-3215, Aug 2010.

[18] K. Jia, T. E. Fischer, and B. Gallois, "Microstructure, hardness and toughness of nanostructured and conventional WC-Co composites," Nanostructured Materials, vol. 10, pp. 875-891, Jul 1998.

[19] M. P. DEvelyn and K. Zgonc, "Elastic properties of polycrystalline cubic boron nitride and diamond by dynamic resonance measurements," Diamond and Related Materials, vol. 6, pp. 812-816, Apr 1997.

[20] D. B. Han and J. J. Mecholsky, "Strength and Toughness Degradation of Tungsten Carbide-Cobalt Due to Thermal-Shock," Journal of the American Ceramic Society, vol. 73, pp. 3692-3695, Dec 1990.

CHAPTER IV

CONCLUSIONS AND FUTURE WORKS

4.1 Conclusions

This project involved completion of number of tasks related to hybrid laser/waterjet machining of PCBN. Specifics of the work are:

1. Achieved cutting of solid PCBN specimen and WC supported PCBN specimen at a high speed and with a good cutting quality.
2. Identified the material removal mechanisms for high thermal conductive PCBN as phase transformation induced stresses lead to controlled fracture.
3. Developed the FEA model for prediction of temperature and stress fields and related laser machining parameters to the fracture characteristics of the material.

In the LWJ cutting of 1.6mm solid PCBN material, experiments are conducted to study the effect of processing parameters on the fracture behaviors. Three different fracture behavior were observed in this experiment and the threshold line energy for through cutting was identified as 11.8kJ/m. Reman spectroscopy results indicated that laser heated PCBN undergoes chemical phase transformation and material separation took place due to the stress induced by volume expansion of the transformed zone. Another set of experiments was conducted on a 4.8mm solid PCBN specimen to obtain the size of phase transformed zone as well as associated expansion strain after laser heating. Measurement of transformation strain and dimensions of transformation region reveals a linear relationship between cutting line energy and transformation depth. The transformation strain was found to be 0.013 through this method. Transformation stress with the obtained expansion strain and transformation

volume was computed in FEM model. Energy release rate for channeling cracks was calculated and compared with experimental result. Good agreement between the analytical result and experimental observation demonstrated the feasibility of proposed mechanism for material separation through controlled crack propagation.

The LWJ Cutting conducted on the 1.6mm tungsten carbide supported PCBN with process parameters of 100in/min and 400W in a single-pass was not successful. The specimen resulted in just a scribing line on the sample surface instead of separating the material. A new method of performing multi-passes defocused beam after the scribing of single-pass focused beam was applied on the double-layer sample that successfully achieved complete cutting. In order to understand the function of the defocused beam, a set of experiments was performed on a 4.8mm thick PCBN piece with 1, 2, 4 and 8 defocused passes after the scribing of focused beam aiming at duplicate the cutting effect during defocused machining without material separation. Spalling cracks happened sometimes and the defocused machining can apparently suppress uncontrolled lateral cracks compared with the focused one.

The numerical analysis of the defocused LWJ cutting of the double-layer WC-PCBN specimen was through the same mechanism as did with solid PCBN sample. Transformation depth was determined from SEM image of cut interface to be 200μm for single-pass cutting and 400 μm for multi-passes defocused cutting. Surface profile measurement determined the best fitting expansion strain to be 0.08 in this sample. Energy release rates of crack propagation were calculated and the degradation of fracture toughness of WC for 20% due to repeated thermal shock was introduced to explain the through-cut result. Initiation of spalling crack was also studied in this specimen. The energy release rate of spalling crack for

three cases were calculated: the single-pass focused cutting, multi-passes defocused cutting and a designed case aiming to reduce lateral cracks. Results indicate that a wider and shallower transformation zone will be benefit to reduce the spalling cracks.

4.2 Future works

Laser machining with other fluid media for thick PCBN specimen

The cutting technique described in this work is laser cutting with waterjet be the assistant medium. Other fluid media such as Nitrogen, Oxygen and Argon would also be possible choices in helping with the cutting. In the cutting of 4.8mm thick PCBN, Nitrogen performed a better work compared with waterjet, which need to be investigated in detail in the future.

Modeling of 2D contour cutting

The 2D contour cutting was successfully performed on PCBN specimen with angle of 120 and 135 degrees. The numerical analysis need to be conducted to identify the processing parameters required for contour cutting of PCBN. Other inserts forms such as a round shape may be also produced through LWJ cutting. Modeling of the round shape cutting is one of the future scopes of work.

LWJ machining of PCD

Polycrystalline diamond (PCD) is another ultra-hard material that suitable to make cutting tools. The LWJ machining method can extend to cutting the PCD specimen. Corresponding experiments and modeling will need to be performed on this new material.

APPENDIX

FEA MODELING OF TEMPERATURE DISTRIBUTION

Modeling method

The laser beam is the high power density surface heat source with Gaussian energy distribution. Numerical analysis was performed in commercial finite element analysis package ABAQUS (Simulia, Providence, RI). Simulation of a movable heat source in ABAQUS requires the implementation of DFLUX subroutines written in FORTRAN programming language, where the heat source power can be determined with desired distribution. The intensity profile of the Gaussian laser beam is described by following equation[1]:

$$I(x,y) = I_0(1 - r_f)\exp\left[-\left(\frac{x}{r}\right)^2 - \left(\frac{y}{r}\right)^2\right] \quad (1)$$

$$I_0 = \frac{P}{\pi r^2}$$

Where I_0 is the peak intensity, P is the laser power, r is the radius of laser spotsize and r_f is the reflectivity of PCBN at 10.6um.The specimens were modeled as rectangular blocks with dimensions 3x10x1.6mm for the WC supported piece and 3x10x4.8mm for the thick PCBN testing piece. Speed of movable heat source was set to be 42.32mm/s, which was the same as actual machining condition. Laser power and laser spotsize were also assigned based on the actual conditions as: P=400W and r=0.1mm for the focused beam and r=0.25mm for the defocused beam. Reflectivity of PCBN at 10.6um was read to be 30% from reported inferred spectrum[2]. Half of the model was considered with assumption of thermal isolation in the plane of symmetry. The boundary conditions applied on the top surface for

waterjet quenching was modeled using a convective heat transfer coefficient h=10000W/($m^2 \cdot K$) reported for forced convection of water flow. The convective coefficient of bottom surface was chosen to be h=50W/($m^2 \cdot K$) for natural air convection. The mechanical and thermal properties of PCBN and WC applied in the model are given in Table 1 and were assumed to be temperature-independent in the analysis.

The temperature field of focused beam for both 1.6mm sample and 4.8mm sample were computed to approximate the depth of transformation zone and valid with SEM images. Temperature field of defocused beam after quenching was also investigated for discussing the thermal-shock effect on fracture toughness degradation of tungsten carbide.

Temperature field solution

The temperature field for both 1.6mm WC-supported sample and 4.8mm solid PCBN sample were calculated for approximation of transformation depth. It was determined based on the assumption that all material heated above a threshold temperature will transform during the cutting process. The transformation temperature of PCBN reported around 1000°C[3] was chosen as the threshold temperature. Temperature distribution across the thickness heated by the laser beam with power distribution described by equations (1) at the time instant of maximum surface temperature for 1.6mm and 4.8mm specimen are presented in Figures 1. Transformation temperature (T=1000 °C) were pointed out, which determined the transformation depth to be 200μm that exactly agreed with experimentally measured value (from SEM Figure). Temperature distribution for 1.6mm piece and 4.8mm piece were almost same indicating that the 4.8mm sample could be a valid replication of the laser effect acted on the 1.6mm piece.

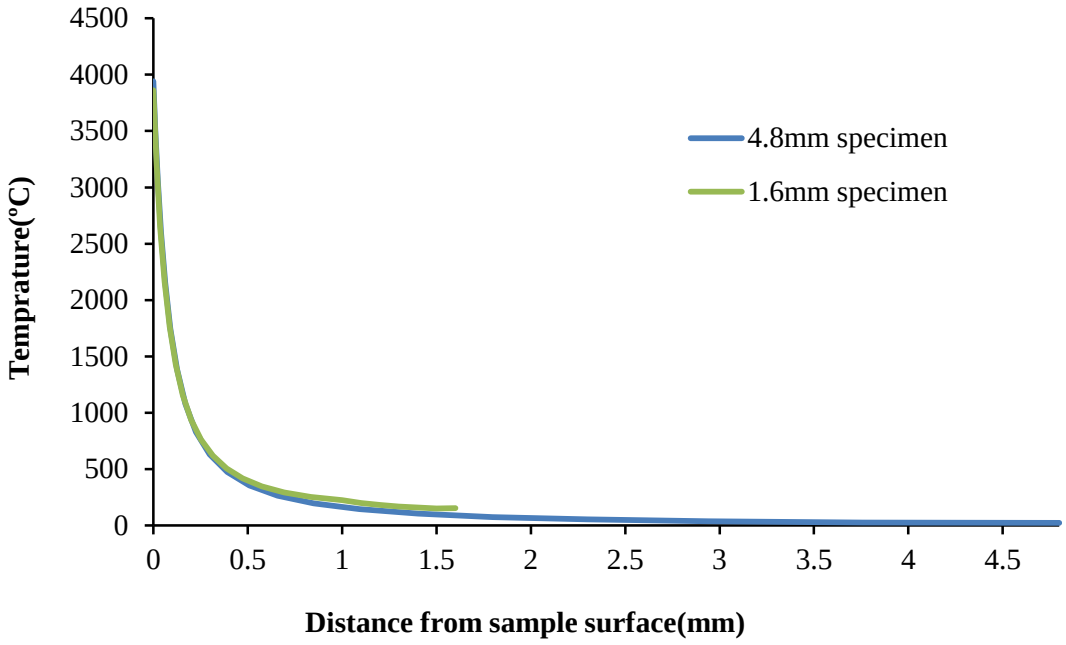

Figure 1. *Temperature distribution across the thickness at the maximum heating instance for both 1.6mm WC-PCBN and 4.8mm solid PCBN with focused beam machining*

. Temperature distribution of the specimen after machined by the defocused beam for 1.6mm specimen are plotted in Figures 2. It can be observed that the tungsten carbide layer could be heated up to about 300-350 °C in each defocused cutting. Water-jet applied following it could be functioned as a thermal shock that can dramatically decrease the fracture toughness of tungsten carbide discovered by other researchers [4-6]

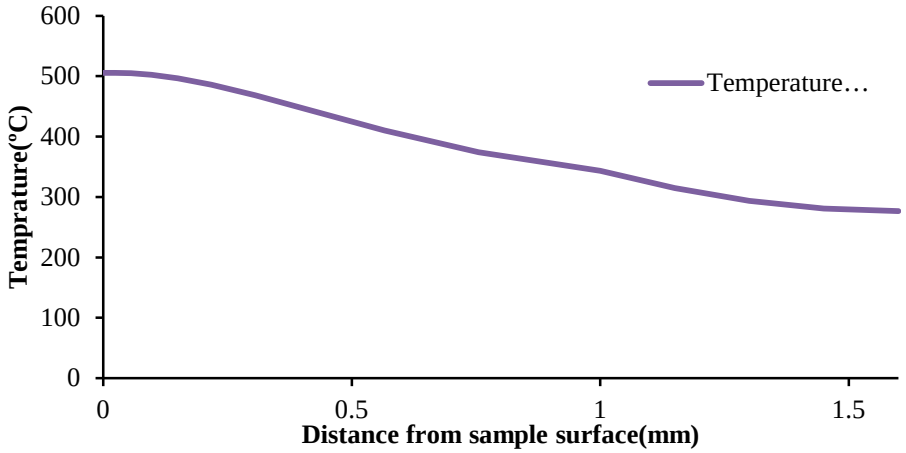

Figure 2. *Temperature distribution across the thickness after machined by the defocused beam for the 1.6mm WC-PCBN*

References

[1] J. E. Moody and R. H. Hendel, "Temperature Profiles Induced by a Scanning Cw Laser-Beam," Journal of Applied Physics, vol. 53, pp. 4364-4371, 1982.

[2] P. J. Gielisse, S. S. Mitra, J. N. Plendl, R. D. Griffis, L. C. Mansur, R. Marshall, et al., "Lattice Infrared Spectra of Boron Nitride and Boron Monophosphide," Physical Review, vol. 155, pp. 1039-&, 1967.

[3] H. Sachdev, R. Haubner, H. Noth, and B. Lux, "Investigation of the cBN/h-BN phase transformation at normal pressure," Diamond and Related Materials, vol. 6, pp. 286-292, Mar 1997.

[4] D. B. Han and J. J. Mecholsky, "Strength and Toughness Degradation of Tungsten Carbide-Cobalt Due to Thermal-Shock," Journal of the American Ceramic Society, vol. 73, pp. 3692-3695, Dec 1990.

[5] W. Acchar, U. U. Gomes, W. A. Kaysser, and J. Goring, "Strength degradation of a tungsten carbide-cobalt composite at elevated temperatures," Materials Characterization, vol. 43, pp. 27-32, Jul 1999.

[6] H. P. S. Sachdev, T. Gera, and P. Nestel, "Effect of iron supplementation on physical growth in children: systematic review of randomised controlled trials," Public Health Nutrition, vol. 9, pp. 904-920, Oct 2006.